Keyvan Hashtrudi-Zaad

Department of Electrical and Computer Engineering
Queen's University
Kingston, Ontario
Canada K7L 3N6
khz@ece.queensu.ca

Septimiu E. Salcudean

Department of Electrical and Computer Engineering
University of British Columbia
Vancouver, British Columbia
Canada V6T 1Z4
tims@ece.ubc.ca

Analysis of Control Architectures for Teleoperation Systems with Impedance/ Admittance Master and Slave Manipulators

Abstract

A large number of bilateral teleoperation control architectures in the literature have been designed based on assumed impedance models of the master and slave manipulators. However, hydraulic or heavily geared and many other manipulators cannot be properly described by impedance models. In this paper, a common four-channel bilateral control architecture designed for the above impedance models is extended to teleoperation systems with master and slave manipulators of either the admittance or impedance type. Furthermore, control parameters that provide perfect transparency under ideal conditions are found for each type of teleoperation system. Because in practice such parameters may not lead to systems that are robust to time delays and model uncertainties, an analysis of the stability and performance robustness of this very general architecture and two-channel architectures is also presented. The analysis uses the passivity-based Llewellyn two-port network absolute stability criterion, as well as bounds on the minimum and range of values of the impedance transmitted to the operator. The results of these evaluations provide design guidelines on choosing a particular control architecture and its parameters given different master and slave manipulator structures.

KEY WORDS—absolute stability, bilateral control, two-port network, teleoperation, transparency

1. Introduction

Teleoperators are designed to enable humans to manipulate dangerous, remote, or delicate tasks via master-slave robotic manipulators with enhanced safety, at lower cost, or even with better accuracy. Teleoperation has found applications in many areas including space technologies, underwater explorations, military/fire-fighting operations, mining, nuclear/toxic waste handling and disposal, surgery, rehabilitation, training, education, and entertainment (Sheridan 1989; Melchiorri and Eusebi 1996).

Besides stability, which is the fundamental requirement for every control system, transparency or telepresence is the principal goal in bilateral teleoperation controller design. Transparency, interpreted as the accurate rendering of the environment to the operator, is technically achieved if the slave position and force follow the master position and force faithfully. Toward this end, several bilateral control architectures have been developed. A survey of most of the proposed architectures can be found in Brooks (1990), Melchiorri and Eusebi (1996), and Salcudean (1998). These architectures can be categorized based on the number and the type of signals transmitted between master and slave. In theory, four-channel (and even three-channel) control architectures that incorporate both master and slave position and force information exchange can offer perfect transparency (Lawrence 1993; Yokokohji and Yoshikawa 1994; Hashtrudi-Zaad and Salcudean 1999). However, in practice, the dynamics of the operator and especially the environment vary drastically, compromising both performance and stability. Moreover, delays in the data transmission channels further complicate the design problem (Lawrence 1993; Salcudean et al. 1995; Daniel and McAree 1998). Therefore, there is a need for guidelines in adjusting the control parameters for a good trade-off between stability robustness and performance.

A majority of the control architectures proposed are tailored for teleoperation systems with impedance types of master and slave manipulators that are driven by "force source"

The International Journal of Robotics Research
Vol. 20, No. 6, June 2001, pp. 419-445,

actuators such as DC motors. In this paper, the 4C bilateral control architecture presented in Lawrence (1993) is extended to teleoperation systems with admittance types of master and/or slave manipulators, and conditions leading to perfect transparency under ideal provisions are presented.

This work uses Llewellyn's absolute stability criterion (Haykin 1970) and the minimum and the dynamic range or Z-width (Colgate and Brown 1994) of the transmitted impedance to the operator to analyze the stability and performance robustness of a number of well-known two-channel and four-channel control architectures given different master and slave manipulator structures. A framework for robust bilateral controller design is then proposed. This approach was inspired by Adams and Hannaford (1999) and addresses robust controller design for haptic interaction.

In this paper, two-port network immittance matrices followed by absolute stability and performance evaluation tools are introduced in Section 2. Dynamic models for four-channel bilateral teleoperation control systems with impedance or admittance types of master and slave manipulators are presented in Section 3. The transparency-optimized control law for an impedance-impedance type of teleoperation system are reviewed and extended to other types of teleoperation systems in Section 4. The evaluation tools introduced in Section 2 are then used in Section 5 to study the trade-offs between stability and performance for two-channel and four-channel control architectures. The above analysis is employed to provide guidelines on tuning bilateral controller parameters for different types of teleoperation systems. Dynamic simulation results are included for verification. Finally, conclusions are drawn in Section 6.

2. Stability Robustness and Performance Evaluation Tools

Consider the block diagram of a teleoperation system as shown in Figure 1, where the master, slave, and communication channel models are lumped into a linear-time-invariant (LTI) master-slave two-port network (MSN) block. The operator and environment are assumed to be in contact with the master and slave and are modeled around their contact-operating point in the Laplace domain by lumped LTI dynamics (Raju, Verghese, and Sheridan 1989; Hannaford 1989a):

$$F_h = F_h^\star - Z_h V_h \quad (1)$$

$$F_e = F_e^\star + Z_e V_e, \quad (2)$$

where Z_h, Z_e, V_h, V_e, F_h, F_e, $F_h^\star$, and $F_e^\star$ are the master and slave impedances and velocities, the operator force on the master, the slave force on the environment, and the exogenous force inputs generated by the operator and the environment, respectively. These LTI models will be employed to study the system performance, whereas the stability analysis tool used in this paper is independent of the operator and environment linearity.

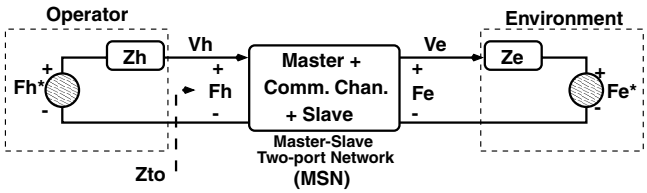

Fig. 1. A teleoperation network block diagram.

Depending on the choice of the network input and output variables $\mathcal{I}$ and $\mathcal{O}$, impedance $\mathcal{Z}$, admittance $\mathcal{Y}$, hybrid $\mathcal{H}$, and inverse hybrid $\mathcal{G}$, network matrices are defined as (Haykin 1970; Adams and Hannaford 1999)

$$\begin{bmatrix} F_h \\ F_e \end{bmatrix} = \mathcal{O}_\mathcal{Z} := \mathcal{Z}\mathcal{I}_\mathcal{Z} = \begin{bmatrix} z_{11} & z_{12} \\ z_{21} & z_{22} \end{bmatrix} \begin{bmatrix} V_h \\ -V_e \end{bmatrix} \quad (3)$$

$$\begin{bmatrix} V_h \\ -V_e \end{bmatrix} = \mathcal{O}_\mathcal{Y} := \mathcal{Y}\mathcal{I}_\mathcal{Y} = \begin{bmatrix} y_{11} & y_{12} \\ y_{21} & y_{22} \end{bmatrix} \begin{bmatrix} F_h \\ F_e \end{bmatrix} \quad (4)$$

$$\begin{bmatrix} F_h \\ -V_e \end{bmatrix} = \mathcal{O}_\mathcal{H} := \mathcal{H}\mathcal{I}_\mathcal{H} = \begin{bmatrix} h_{11} & h_{12} \\ h_{21} & h_{22} \end{bmatrix} \begin{bmatrix} V_h \\ F_e \end{bmatrix} \quad (5)$$

$$\begin{bmatrix} V_h \\ F_e \end{bmatrix} = \mathcal{O}_\mathcal{G} := \mathcal{G}\mathcal{I}_\mathcal{G} = \begin{bmatrix} g_{11} & g_{12} \\ g_{21} & g_{22} \end{bmatrix} \begin{bmatrix} F_h \\ -V_e \end{bmatrix}, \quad (6)$$

where each of the above matrices, if they exist, can be found given any of the other matrices. The above representations fall into the immittance category defined as $\mathcal{P}_\mathcal{P} := \mathcal{O}_\mathcal{P}\,\mathcal{I}_\mathcal{P}$, $\mathcal{P} = [p_{ij}]$ $i, j = 1, 2$, in which $\mathcal{O}_\mathcal{P}^T\mathcal{I}_\mathcal{P} = \mathcal{O}_\mathcal{Z}^T\mathcal{I}_\mathcal{Z} = \mathcal{O}_\mathcal{Y}^T\mathcal{I}_\mathcal{Y} = \mathcal{O}_\mathcal{H}^T\mathcal{I}_\mathcal{H} = \mathcal{O}_\mathcal{G}^T\mathcal{I}_\mathcal{G} = F_hV_h - F_eV_e$ is the instantaneous power delivered to the MSN. Hence, the class of immittance representations is of particular interest to the energy-based stability analysis tools such as passivity theory.

Passivity theory has been employed to design passive MSNs (Raju, Verghese, and Sheridan 1989; Anderson and Spong 1989; Lawrence 1993) that render the teleoperation system passive and stable when terminated by strictly passive operator and environment dynamics. Passivity of the MSN is a conservative condition. Instead, a structured singular value condition (Colgate 1993) or absolute stability condition (Adams and Hannaford 1999) guarantees stability in a nonconservative way by ensuring passivity of the one-port networks resulted from terminating the MSN by *any* passive environment and operator. Llewellyn's absolute stability condition is expressed in terms of the MSN immittance matrices in the following (Haykin 1970):

An LTI two-port network is absolutely stable if and only if

- p_{11} and p_{22} are positive real and
- the inequality

$$\eta_\mathcal{P}(\omega) := -\frac{\Re\{p_{12}p_{21}\}}{|p_{12}p_{21}|} + 2\frac{\Re\{p_{11}\}\Re\{p_{22}\}}{|p_{12}p_{21}|} \geq 1 \quad (7)$$

holds on the $j\omega$ axis for all $\omega \geq 0$, where $\eta_{\mathcal{P}}(\omega)$ is called the network stability parameter and $|\cdot|$ and $\Re\{\cdot\}$ denote the absolute and real values of their corresponding arguments.

The positive realness of p_{11} and p_{22} implies passivity of the master and slave when there is no coupling between them, that is, when $p_{12} = p_{21} = 0$. This can also be viewed as the passivity of the master and slave when they are free or clamped. On the other hand, condition (7) incorporates the effect of coupling. After expanding the positive realness condition, Llewellyn's absolute stability conditions are equivalent to the following conditions:

- the immittance parameters p_{11} and p_{22} have no poles in the open right-half-plane (RHP),
- any poles of p_{11} and p_{22} on the imaginary axis are simple and have real and positive residues , and
- the inequalities

$$\Re\{p_{11}\} \geq 0 \quad (8)$$

$$\eta_{\mathcal{P}}(\omega) = -\cos(\angle p_{12}p_{21}) + 2\frac{\Re\{p_{11}\}\Re\{p_{22}\}}{|p_{12}p_{21}|} \geq 1 \quad (9)$$

hold, where $\cos(\angle Z) := \frac{\Re\{Z\}}{|Z|}$ for any complex Z. Llewellyn's criterion is valid for any member of the immittance class, and moreover the value of the stability parameter is independent of the immittance matrix employed, that is, $\eta_{\mathcal{Y}} = \eta_{\mathcal{Z}} = \eta_{\mathcal{H}} = \eta_{\mathcal{G}}$ (Haykin 1970). This property will be used in Section 5 to compare the stability parameters of different two-channel control architectures. In fact, to simplify the stability analysis, the stability parameter for each architecture will be expressed in terms of a different network matrix.

Absolute stability depends on the network parameters alone and is not subject to the operator or environment linearity. A system that is not absolutely stable (i.e., if any of the above conditions is not satisfied) is called potentially unstable (Haykin 1970; Adams and Hannaford 1999), implying that there exists a particular pair of passive operator and environment that destabilizes the system. However, this does not mean that a potentially unstable system is necessarily unstable.

Hogan (1989) has shown that the human arm impedance is highly adaptable and time varying, and although the muscular actuators and the neural feedback driving the arm are active systems, the human hand shows passive characteristics. Therefore, the operator can be modeled by a state independent (exogenous) input force and a passive impedance as in (1) (Colgate and Hogan 1988). As for the environment, most of the objects with which we interact are passive and absorb energy. Because the dynamic range of the operator impedance is not as wide as that of the environment, and in some cases the upper bound on the impedance of the object to be manipulated is known a priori, the above absolute stability analysis may provide us with conservative stability conditions. To find more relaxed conditions, one can replace the operator or environment impedance by an ideal impedance with infinite dynamic range shunted with an impedance equal to the operator or environment maximum impedance value, respectively. Then, one may proceed by absorbing the shunt impedance into the MSN and applying Llewellyn's criterion to the new two-port network as described in Appendix A.

After stability, transparency is the principal goal of teleoperation control system design. Transparency can be described quantitatively as a match between the environment impedance and the impedance transmitted to the operator; that is, $Z_{to} := \frac{F_h}{V_h}|_{F_e^\star=0} = \frac{F_e}{V_e}|_{F_e^\star=0} := Z_e$ (Lawrence 1993). Using (1)-(2) and (5), Z_{to} can be expressed in terms of the MSN hybrid parameters as

$$Z_{to} = \frac{h_{11} + \Delta h \cdot Z_e}{1 + h_{22}Z_e}, \quad (10)$$

where $\Delta h := h_{11}h_{22} - h_{12}h_{21}$. If the hybrid parameters are not functions of Z_h and Z_e, perfect transparency can be achieved if

$$h_{11} = h_{22} = 0 \quad \text{Transparency} \quad (11)$$

$$h_{12} = -h_{21} = 1 \quad \text{Condition-set} \quad (12)$$

is satisfied (Hannaford 1989a). Hence, a perfectly transparent system is marginally absolutely stable, as $\Re\{h_{11}\} = 0$ and $\eta_{\mathcal{H}} = 1$ in (8)-(9). Therefore, to have higher stability robustness, perfect transparency has to be compromised. In addition, due to the presence of significant transmission delay, there is a trade-off between stability and performance; consequently, perfect transparency is not attainable in practice (Hannaford 1989b; Lawrence 1993; Salcudean et al. 1995). Therefore, one should examine Z_{to} for the infinite spectrum of the environment impedance to evaluate system transparency, which is an involved process. To ease the burden and to quantify transparency, Z_{to} is examined for extreme values of Z_e, that is, when the slave is in free motion ($Z_e = 0$) or clamped ($Z_e \to \infty$). If the network parameters are not functions of Z_h and Z_e, the minimum value and dynamic range of the transmitted impedance can be evaluated as follows:

$$Z_{tomin} := Z_{to}|_{Z_e=0} = h_{11} \quad (13)$$

$$Z_{towidth} := Z_{to}|_{Z_e\to\infty} - Z_{tomin} = \frac{-h_{12}h_{21}}{h_{22}}. \quad (14)$$

Here, the notion of Z-width is borrowed from haptic literature (Colgate and Brown 1994) to express the dynamic range of the impedance transmitted to the operator while maintaining stability. The choice of Z-width is compliant with its original definition in Colgate and Brown (1994) as Llewellyn's criterion guarantees passivity of the transmitted impedance. Good performance is then characterized by $|Z_{tomin}| \to 0$ and $|Z_{towidth}| \to \infty$.

The above analysis and evaluation tools will be used later to assess stability and performance of a number of commonly used bilateral control architectures when applied to different types of teleoperation systems as categorized by properties of their master and slave manipulators.

3. Teleoperation System Types

In general, manipulators can be categorized as being devices of the admittance or impedance type, depending on whether they behave like velocity or force sources, respectively. This behavior is determined by the structural design and actuation employed by the manipulator. By definition, an impedance device receives a force command and applies force to its environment in response to its measured position (Adams and Hannaford 1999). For example, magnetically levitated wrists (Hollis, Salcudean, and Allan 1991) and SensAble's Phantom (Massie and Salisbury 1994) are among the devices that possess high back-drivability and low impedance. On the other hand, an admittance device receives a velocity/position command and applies a velocity/position to its environment in response to its measured contact force. As an example, a heavily geared Puma robot (Clover et al. 1997) or hydraulic robots such as excavators (Salcudean et al. 1998) are admittance devices with low back-drivability and low compliance.

By closing a properly designed position or force control loop around a device, it is possible to change the manipulator type from impedance to admittance or vice versa, as viewed from outside of the control loop. However, this change is limited by robustness considerations. Throughout this paper, the LTI dynamic models

$$Z_m V_h = F_h + F_{cm} \quad \text{Impedance Master} \quad (15)$$
$$Z_s V_e = -F_e + F_{cs} \quad \text{Impedance Slave} \quad (16)$$
$$Y_m F_h = V_h + V_{cm} \quad \text{Admittance Master} \quad (17)$$
$$Y_s F_e = -V_e + V_{cs} \quad \text{Admittance Slave} \quad (18)$$

are used for impedance/admittance types of master and slave manipulators, where Z_m, Z_s, Y_m, Y_s and $F_{cm}, F_{cs}, V_{cm}, V_{cs}$ denote the master and slave dynamics and their control inputs. Z_m, Z_s and Y_m, Y_s are typically low impedance and admittance dynamics, respectively.

Based on the above manipulator categories, there exist four different types of teleoperation systems: impedance-impedance, impedance-admittance, admittance-impedance, and admittance-admittance. Figure 2 shows the block diagram of the four types of teleoperation systems controlled by general 4C bilateral controllers. T_d denotes the communication channel time delay, and the C and E blocks denote the control compensator transfer functions.

In all four bilateral controllers, there are generally two types of control signals applied to the master and slave actuators. One type is from local controllers, that is, C_5, C_6, C_m, C_s and E_5, E_6, E_m, E_s, built around the master and slave. The other is from feedforward controllers, that is, $C_1, \cdots, C_4$ and $E_1, \cdots, E_4$, sending signals to the remote site. The feedforward control signals applied to the master or slave can be of either position or force type, which is determined by the type of the manipulator. For example, the feedforward signal to an impedance device has to be of the force type. This signal can be either the remote site measured contact force (e.g., $C_2 F_e$ or $C_3 F_h$) or the coordinating force created by passing the remote manipulator measured position through an impedance-type filter (e.g., $C_1 V_h$ or $C_4 V_e$). In a dual way, the feedforward signal to an admittance device has to be a measured position (e.g., $E_2 V_e$ or $E_3 V_h$) or the coordinating position created by passing the remote measured contact force through an admittance-type filter (e.g., $E_1^{-1} F_h$ or $E_4^{-1} F_e$).

Table 1 provides a typical description and model of the subsystem blocks assumed in this paper. The force control parameters C_2, C_3, C_5, C_6 and the position control parameters E_2, E_3, E_5, E_6 are assumed to be scalar gains. This assumption allows for the analytical study of the system stability parameter $\eta_{\mathcal{P}}$ introduced in (9). If these parameters are frequency dependent, then a numerical study has to be performed instead of a qualitative analysis to examine the trade-offs between performance and stability. To avoid introducing new parameters, no specific models are presented for Y_m, Y_s, E_m, and E_s. Instead, all the mathematical derivations in Sections 4 and 5 will be concerned with the impedance-impedance type system of Figure 2a. A mapping will be provided to find equivalent relationships for systems with admittance master and/or slave. For controller performance evaluation, Z_h and Z_e are modeled by LTI systems in this paper. The stability analysis does not change if the operator and environment are modeled as nonlinear passive systems.

4. Four-Channel Architectures and Transparency-Optimized Control Laws

In the following, the four-channel bilateral control architecture for the impedance-impedance teleoperation system of Figure 2a is considered. Conditions on the control parameters leading to perfect transparency under ideal provisions are derived. The results for impedance-admittance, admittance-impedance, and admittance-admittance teleoperation systems are summarized in Appendix B.

4.1. Impedance-Impedance Type of Teleoperation Systems

After applying the control commands F_{cm} and F_{cs} to the impedance-impedance system of Figure 2a, the dynamics of the closed-loop system are expressed as

$$Z_{cm} V_h + C_4 e^{-sT_d} V_e = (1 + C_6) F_h - C_2 e^{-sT_d} F_e \quad (19)$$
$$Z_{cs} V_e - C_1 e^{-sT_d} V_h = C_3 e^{-sT_d} F_h - (1 + C_5) F_e, \quad (20)$$

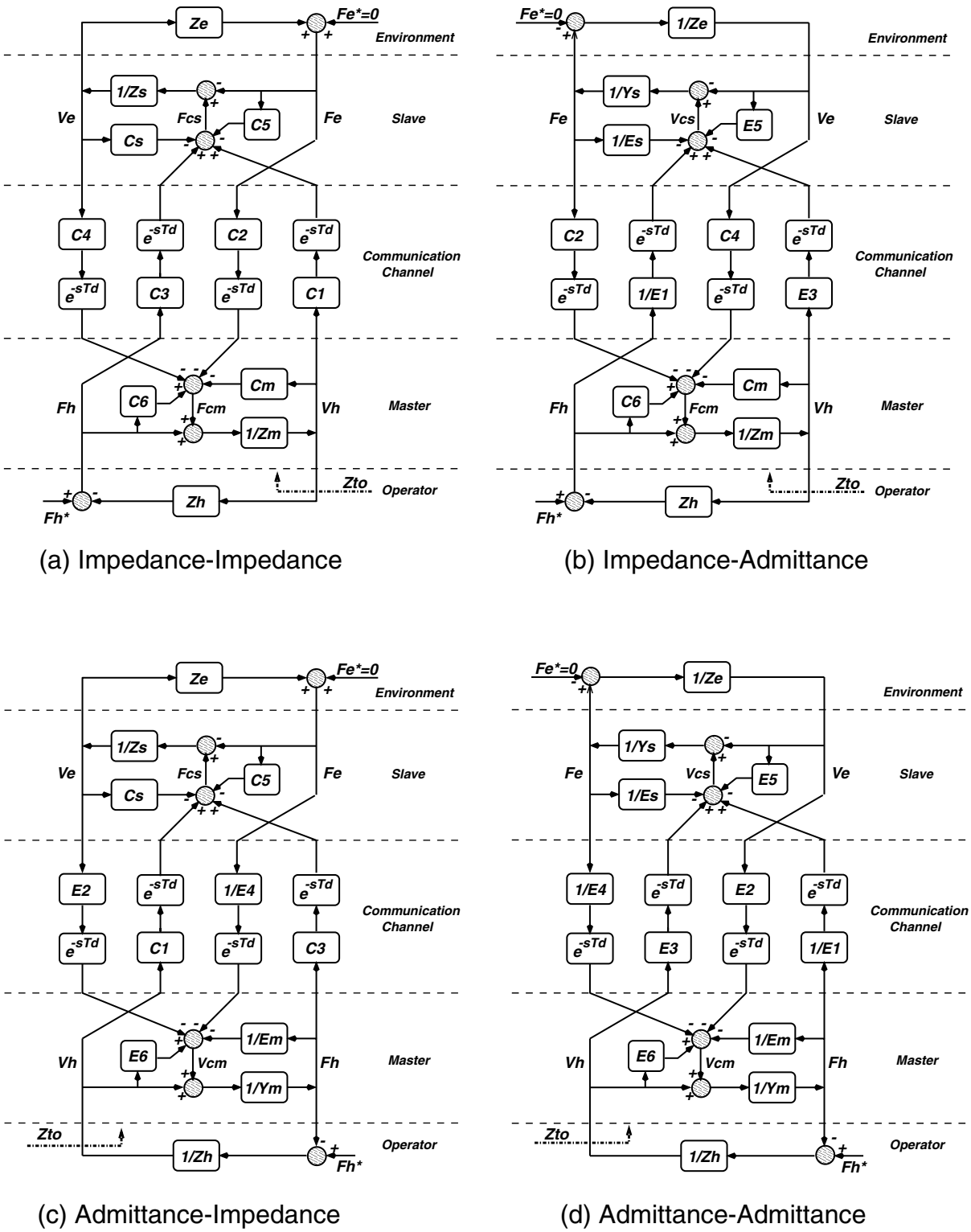

Fig. 2. Block diagrams of four types of teleoperation systems controlled by general four-channel bilateral controllers.

Table 1. Nomenclature and Typical Description of Subsystems in the General Bilateral Teleoperation Control Systems of Figure 2 (the Models Used for the Analysis Given in Sections 4 and 5 Are Described by Transfer Functions in the Laplace Domain)

Block	Description	Model
Impedance models of master and slave		
Z_m	Master impedance	Mass, $M_m s$
Z_s	Slave impedance	Mass, $M_s s$
C_m	Master local position controller	Damper spring, $B_m + \frac{K_m}{s} s$
C_s	Slave local position controller	Damper spring, $B_s + \frac{K_s}{s}$
C_1	Master coordinating force feedforward controller	Impedance filter
C_2	Slave force feedforward controller	Scalar gain
C_3	Master force feedforward controller	Scalar gain
C_4	Slave coordinating force feedforward controller	Impedance filter
C_5	Slave local force controller	Scalar gain
C_6	Master local force controller	Scalar gain
Admittance models of master and slave		
Y_m	Master admittance	Admittance transfer function
Y_s	Slave admittance	Admittance transfer function
E_m	Master local force controller	Impedance filter
E_s	Slave local force controller	Impedance filter
E_1	Master coordinating position feedforward controller	Impedance filter
E_2	Slave position feedforward controller	Scalar gain
E_3	Master position feedforward controller	Scalar gain
E_4	Slave coordinating position feedforward controller	Impedance filter
E_5	Slave local position controller	Scalar gain
E_6	Master local position controller	Scalar gain
Operator and environment		
Z_h	Operator impedance	Impedance transfer function
Z_e	Environment impedance	Impedance transfer function
$F_h^\star$	Operator exogenous force input	-
$F_e^\star$	Environment exogenous force input	0

where $\underline{Z_{cm} := Z_m + C_m}$ and $\underline{Z_{cs} := Z_s + C_s}$. To analyze system stability and performance, one needs the MSN hybrid parameters. These parameters can be derived in terms of the system and control parameters from (5) and (19)-(20) as

$$h_{11} = \frac{Z_{cm}Z_{cs} + C_1C_4e^{-2sT_d}}{(1+C_6)Z_{cs} - C_3C_4e^{-2sT_d}} \tag{21}$$

$$h_{12} = \frac{C_2Z_{cs}e^{-sT_d} - C_4(1+C_5)e^{-sT_d}}{(1+C_6)Z_{cs} - C_3C_4e^{-2sT_d}} \tag{22}$$

$$h_{21} = -\frac{C_3Z_{cm}e^{-sT_d} + C_1(1+C_6)e^{-sT_d}}{(1+C_6)Z_{cs} - C_3C_4e^{-2sT_d}} \tag{23}$$

$$h_{22} = \frac{(1+C_5)(1+C_6) - C_2C_3e^{-2sT_d}}{(1+C_6)Z_{cs} - C_3C_4e^{-2sT_d}}. \tag{24}$$

Using (10) and (21)-(24), the operator-transmitted impedance is obtained as

$$Z_{to} = \frac{(Z_{cm}Z_{cs} + C_1C_4e^{-2sT_d}) + [(1+C_5)Z_{cm} + C_1C_2e^{-2sT_d}]Z_e}{[(1+C_6)Z_{cs} - C_3C_4e^{-2sT_d}] + [(1+C_5)(1+C_6) - C_2C_3e^{-2sT_d}]Z_e} \tag{25}$$

If the time delay T_d is negligible, using

$$\begin{cases} C_1 = Z_{cs} \\ C_2 = 1 + C_6 \\ C_3 = 1 + C_5 \\ C_4 = -Z_{cm} \end{cases} \quad \begin{array}{c} \text{Impedance-impedance} \\ \text{Transparency-optimized} \\ \text{Control law} \end{array} \tag{26}$$

and $(C_2, C_3) \neq (0, 0)$, known as the transparency-optimized control law, satisfies (11)-(12) to provide perfect transparency (Lawrence 1993; Hashtrudi-Zaad and Salcudean 1999). The physical interpretation of (26) is that in order to achieve transparency, the master and slave dynamics have to be canceled out using inverse dynamics and the forces fed forward have to match the net forces exerted by the operator and the environment. In this case, the master and slave are effectively removed and the operator and the environment are virtually connected. Because in practice, acceleration signals are not available or are too noisy, only the master and slave positions and velocities are transmitted, that is, $C_1 = C_s = B_s + \frac{K_s}{s}$ and $C_4 = -C_m = -(B_m + \frac{K_m}{s})$.

As for stability of the transparency-optimized four-channel controller, the system characteristic equation under ideal conditions is

$$\Delta_0 = (C_2Z_{cs} + C_3Z_{cm})(Z_h + Z_e) = 0. \tag{27}$$

This indicates that if C_2 and C_3 are single gains and the operator and environment are passive, the system remains stable if $C_2 > -\min(\frac{M_m}{M_s}, \frac{B_m}{B_s}, \frac{K_m}{K_s})C_3$ holds. In terms of stability robustness, although this system is stable for $C_2, C_3 > 0$, because $h_{11} = h_{22} = 0$ and $h_{12} = -h_{21} = 1$, the system absolute stability is marginal as $\eta = 1$. Note that because the term $C_2Z_{cs} + C_3Z_{cm}$ is present in the denominator of h_{11} and h_{22} for $T_d \approx 0$, it cannot have roots in the RHP to be used in Llewellyn's conditions (8)-(9).

In the absence of time delays, the analysis of stability and performance is straightforward and stable perfect transparency is achievable. However, when significant delays are present, both stability and transparency are compromised and their analysis becomes too involved. Instead, one can use the analysis tools introduced in Section 2 to numerically evaluate stability robustness and transparency performance for different control architectures.

5. Stability and Performance Analysis and Evaluation of Two-Channel and Four-Channel Control Architectures

The four-channel control architectures presented in Figure 2 are simplified if only one signal—position or force—is transmitted from the master or slave. Four two-channel control architectures are possible, named for the variable measured and sent to the remote site: force-force (F-F), position-position (P-P), force-position (F-P), and position-force (P-F). Two-channel architectures have been reported in a number of papers (Handlykken and Turner 1980; Hannaford and Anderson 1988; Raju, Verghese, and Sheridan 1989; Anderson and Spong 1989; Brooks 1990; Kazerooni, Tsay, and Hollerbach 1993). Because they require fewer sensors and are less complicated, two-channel architectures are desirable. In addition, due to the simplifications provided by eliminating two out of four data transmission channels, the analytical study of the two-channel architectures is easily done. The analysis in this section is aimed at providing the teleoperation control system designer with an initial choice of control architecture and parameters based on the type of master and slave.

In this section, the stability and performance of an impedance-impedance type of teleoperation system controlled by two-channel controllers is discussed in the presence of significant delays. To cover for the other three types, it is assumed that the local position controllers are tight enough to create admittance master and/or slave with any desired admittance. This assumption can be justified by considering the dynamics and the control applied to an impedance device, say the slave. The slave closed-loop dynamics (20) can be rearranged as

$$\frac{1}{Z_{cs}}F_e = -V_e + \frac{1}{Z_{cs}}[-C_5F_e + C_1e^{-sT_d}V_h + C_3e^{-sT_d}F_h]. \tag{28}$$

Comparing (28) with the dynamics of an admittance-type slave in (18), one concludes at $Y_s = \frac{1}{Z_{cs}}$ and $V_{cs} =$

Table 2. Parameter Mapping That Allows for the Analysis of Impedance-Admittance, Admittance-Impedance, and Admittance-Admittance Teleoperation Systems Using Mathematical Derivations (Such As Network Parameters, Transmitted Impedance, Stability Parameter) Obtained for an Impedance-Impedance System

Master			Slave		
Impedance		**Admittance**	**Impedance**		**Admittance**
Z_{cm}	$\longleftrightarrow$	$1+E_6$	Z_{cs}	$\longleftrightarrow$	$1+E_5$
C_4	$\longleftrightarrow$	E_2	C_1	$\longleftrightarrow$	E_3
C_2	$\longleftrightarrow$	E_4^{-1}	C_3	$\longleftrightarrow$	E_1^{-1}
$1+C_6$	$\longleftrightarrow$	Y_{em}	$1+C_5$	$\longleftrightarrow$	Y_{es}

$\frac{1}{Z_{cs}}(-C_5F_e+C_1e^{-sT_d}V_h+C_3e^{-sT_d}F_h)$. If the slave local position feedback is needed, then part of C_sV_e can be kept in V_{cs}. It is clear that if Z_{cs} is assumed to be high, then $\frac{1}{Z_{cs}}$ can represent the low admittance of an admittance device, the amount of which can appropriately be controlled by a local position controller C_s. Also, in case an impedance-type representation of an admittance master and/or slave as presented in (28) is not possible, the robustness analysis equations for the other three types of teleoperation systems are easily achievable. This can be done by substituting for $C_1,\cdots,C_6$ and Z_{cm} and Z_{cs} from Table 2 in the analytical equations that will be derived for an impedance-impedance type of system in Section 5.1. Note that $\underline{Y_{em}:=Y_m+E_m^{-1}}$ and $\underline{Y_{es}:=Y_s+E_s^{-1}}$.

5.1. Two-Channel Control Architectures

In the following, the stability robustness and performance evaluation tools introduced in Section 2 will be employed to analyze the two commonly used two-channel control architectures P-P and F-P. The results for the F-F and P-F control architectures are presented in Appendix C.

5.1.1. Position-Position Control Architecture

Position-position (P-P) is the first bilateral control architecture that was implemented in the 1950s. In this control architecture, which was further developed and analyzed in Raju, Verghese, and Sheridan (1989), Anderson and Spong (1989), Niemeyer and Slotine (1991), and Salcudean, Wong, and Hollis (1995), the direct force feedforward terms are set to zero; that is, $C_2=C_3=0$. For this controller, the hybrid parameters in (21)-(24) are

$$h_{11}=\frac{Z_{cm}Z_{cs}+C_1C_4e^{-2sT_d}}{(1+C_6)Z_{cs}},\quad h_{12}=\frac{-C_4(1+C_5)e^{-sT_d}}{(1+C_6)Z_{cs}}$$
$$h_{21}=-\frac{-C_1e^{-sT_d}}{Z_{cs}},\quad h_{22}=\frac{(1+C_5)}{Z_{cs}}. \tag{29}$$

To study system stability robustness, one needs to evaluate the MSN stability parameter in (9) by substituting the immittance parameters with the hybrid ones. Because h_{11} is the sum of two terms, one of which is delay dependent, it is too difficult to analytically study the system absolute stability using the hybrid representation. Among other network matrices, the impedance parameters that can be found from the hybrid parameters are not directly a function of h_{11}. Instead, because the value of the stability parameter is independent of the type of the network matrix used, that is, $\eta_{\mathcal{H}}=\eta_{\mathcal{Z}}$, the impedance parameters

$$z_{11}:=\frac{\Delta h}{h_{22}}=\frac{Z_{cm}}{1+C_6},\quad z_{12}:=\frac{h_{12}}{h_{22}}=\frac{-C_4e^{-sT_d}}{1+C_6}$$
$$z_{21}:=\frac{-h_{12}}{h_{22}}=\frac{C_1e^{-sT_d}}{1+C_5},\quad z_{22}:=\frac{1}{h_{22}}=\frac{Z_{cs}}{1+C_5} \tag{30}$$

are used in (9) to yield

$$\eta_{pp}(\omega)=\eta_{pp1}+\eta_{pp2}=-\cos(\angle\frac{-C_1C_4e^{-j2\omega T_d}}{(1+C_5)(1+C_6)})$$
$$+2\frac{\Re\{\frac{Z_{cm}}{1+C_6}\}\Re\{\frac{Z_{cs}}{1+C_5}\}}{|\frac{C_1C_4e^{-j2\omega T_d}}{(1+C_5)(1+C_6)}|} \tag{31}$$
$$=sgn((1+C_5)(1+C_6))[-\cos(\angle-C_1C_4e^{-j2\omega T_d})$$
$$+2\frac{\Re\{Z_{cm}\}\Re\{Z_{cs}\}}{|C_1C_4|}]. \tag{32}$$

Because $|e^{-j2\omega T_d}|=1$, η_{pp2} is independent of delay. Thus, the effect of delay on system stability is restricted to only one term, that is, η_{pp1}. Because $\eta_{pp1}\in[-1,1]$, and it includes $e^{j2\omega T_d}$, the absolute stability of the system can be guaranteed only when $\eta_{pp2}\geq 2$, that is, $sgn((1+C_5)(1+C_6))|C_1C_4|\leq \Re\{Z_{cm}\}\Re\{Z_{cs}\}$. This shows that there has to be a minimum amount of damping in the master and slave. To reduce damping at the master while maintaining absolute stability, the amount of damping has to be increased at the slave and vice versa. In addition, higher damping or velocity feedback at the master and slave and lower coordinating force feedforward enhances system absolute stability. However, because $\Re\{Z_{cm}\}\Re\{Z_{cs}\}$ is not frequency dependent, but $|C_1C_4|$ is, the above condition is implementable only for some range of

frequencies; therefore, η_{pp} cannot be ≥ 1 for all frequencies. The effect of local position feedback on stability robustness is more significant than the effect of local force feedback. This is caused by the master and slave sending out only position signals, and intuitively positions are primarily controlled by position controllers. As for the second condition of absolute stability, the passivity of the uncoupled master (z_{11}) and slave (z_{22}) is guaranteed because Z_{cm} and Z_{cs} are passive.

To investigate performance, (13)-(14) are used to obtain

$$\begin{aligned} Z_{tomin} &= \frac{Z_{cm}}{1+C_6} - Z_{towidth} \\ Z_{towidth} &= \frac{-C_1 C_4 e^{-2sT_d}}{(1+C_6)Z_{cs}}. \end{aligned} \tag{33}$$

Attenuation of the force feedforward parameters C_1 and C_4 to enhance stability robustness in (32) degrades performance as $Z_{towidth}$ decreases. This behavior clearly shows the compromise between stability and performance in terms of the feedforward parameters. On the other hand, allowing larger local force feedback parameters C_6 has a mixed effect on performance Z_{tomin} and $Z_{towidth}$ as both decrease. Finally, a decrease in local position feedback parameters C_m and C_s enhances performance in free motion and transparency bandwidth at the cost of degraded stability robustness. By comparing (33) with (51) of the F-F architecture in Appendix C, one can note that Z_{tomin} is lower for the P-P architecture. In fact, $(Z_{towidth})_{ff} = (Z_{tomax})_{pp}$.

If the transparency-optimized law (26) is used in choosing $C_1 = Z_{cs}$ and $C_4 = -Z_{cm}$, the conventional P-P architecture is implemented (Lawrence 1993), and η_{pp} simplifies to

$$\begin{aligned} \eta_{pp}(\omega) = sgn((1+C_5)(1+C_6))[&-\cos(\angle Z_{cm} Z_{cs} e^{-j2\omega T_d}) \\ &+ 2\cos(\angle Z_{cm})\cos(\angle Z_{cs})]. \end{aligned} \tag{34}$$

In this case, η_{pp} is neither a function of the force feedforward parameters nor a strong function of the master and slave damping terms $\Re\{Z_{cm}\}\Re\{Z_{cs}\}$. The only way to slightly improve the stability robustness is through $\cos(\angle Z_{cm})$ and $\cos(\angle Z_{cs})$ by increasing the relative amount of damping in the master and slave dynamics. Figure 3 shows the effect of damping and stiffness on $\cos(\angle Z)$. As damping increases, the curve flattens out, making the system more robust, whereas an increase in stiffness increases the peak frequency and narrows the frequency response. If the time delay is negligible, by using hybrid parameters it is possible to show that $\eta_{pp} = sgn(\frac{1}{(1+C_5)(1+C_6)})\cos(\angle \frac{Z_{cm}}{Z_{cs}}) \leq 1, \forall \omega \geq 0$ and $Z_{tomin} \to 0$, implying good performance when operating on soft objects or in free motion at the cost of potential instability. The frequency ω_o at which η_{pp} is maximized is determined from $\frac{B_m}{B_s} = \frac{M_m \omega_o - \frac{K_m}{\omega_o}}{M_s \omega_o - \frac{K_s}{\omega_o}}$. In this case, the stability parameter flattens out to unity at all frequencies; that is, the system is marginally absolutely stable if and only if $\frac{M_m}{M_s} = \frac{B_m}{B_s} = \frac{K_m}{K_s}$ holds. This can be achieved by proper selection of the local position control parameters for impedance devices and local force control parameters for admittance devices (recall from Table 2 that Z_{cm} maps to $1 + E_6$ for admittance devices).

5.1.2. Force-Position Control Architecture

The force-position (F-P) control architecture, also known as flow forward or force feedback, has been developed, implemented, and analyzed by many researchers for the past two decades (Handlykken and Turner 1981; Hannaford and Anderson 1988; Lawrence 1993; Leung, Francis, and Apkarian 1995). In this architecture, direct force feedforward from the master to the slave and coordinating force feedfoward from the slave to the master are removed; that is, $C_3 = C_4 = 0$. From (21)-(24), the hybrid parameters

$$\begin{aligned} h_{11} &= \frac{Z_{cm}}{1+C_6}, \qquad h_{12} = \frac{C_2 e^{-sT_d}}{1+C_6}, \\ h_{21} &= \frac{-C_1 e^{-sT_d}}{Z_{cs}}, \quad h_{22} = \frac{1+C_5}{Z_{cs}} \end{aligned} \tag{35}$$

are obtained whereas the stability parameter is given by

$$\begin{aligned} \eta_{fp}(\omega) := \eta_{fp1} + \eta_{fp2} &= \cos(\angle \frac{C_1 C_2 e^{-j2\omega T_d}}{(1+C_6)Z_{cs}}) \\ &+ 2\frac{\Re\{\frac{Z_{cm}}{1+C_6}\}\Re\{\frac{1+C_5}{Z_{cs}}\}}{|\frac{-C_1 C_2 e^{-j2\omega T_d}}{(1+C_6)Z_{cs}}|} \end{aligned} \tag{36}$$

$$\begin{aligned} &= sgn(1+C_6)[\cos(\angle \frac{C_1 C_2 e^{-j2\omega T_d}}{Z_{cs}}) \\ &+ 2\frac{(1+C_5)\Re\{Z_{cm}\}}{|C_1 C_2|}\cos(\angle \frac{1}{Z_{cs}})], \end{aligned} \tag{37}$$

where $\cos(\angle \frac{1}{Z}) = \cos(\angle Z)$. Similar to the P-P architecture, the absolute stability condition (9) is met over a certain range of frequencies in which $\eta_{fp2} \geq 2$, that is, when $(1+C_5)\Re\{Z_{cm}\} \geq sgn(1+C_6)|C_1 C_2|$. This implies that to increase stability robustness, master damping (Hannaford and Anderson 1988) and slave local force feedback should be amplified (i.e., higher master and lower slave impedances) (Hannaford 1989b), whereas force feedforward should be attenuated. This suggests that in terms of stability robustness, the F-P architecture is suitable for an admittance-impedance type of teleoperation system. To guarantee absolute stability for a broad range of frequencies, the feedforward control parameter C_2 has to be a low-pass filter instead of a constant as assumed in Table 1. This is because at high frequencies, $\cos(\angle \frac{1}{Z_{cs}}) = \cos(\angle Z_{cs}) \to 0$, as shown in Figure 3, and as a result η_{fp2} converges to zero. In this case, (37) is no longer valid and (36) has to be used instead. Note from (37) that

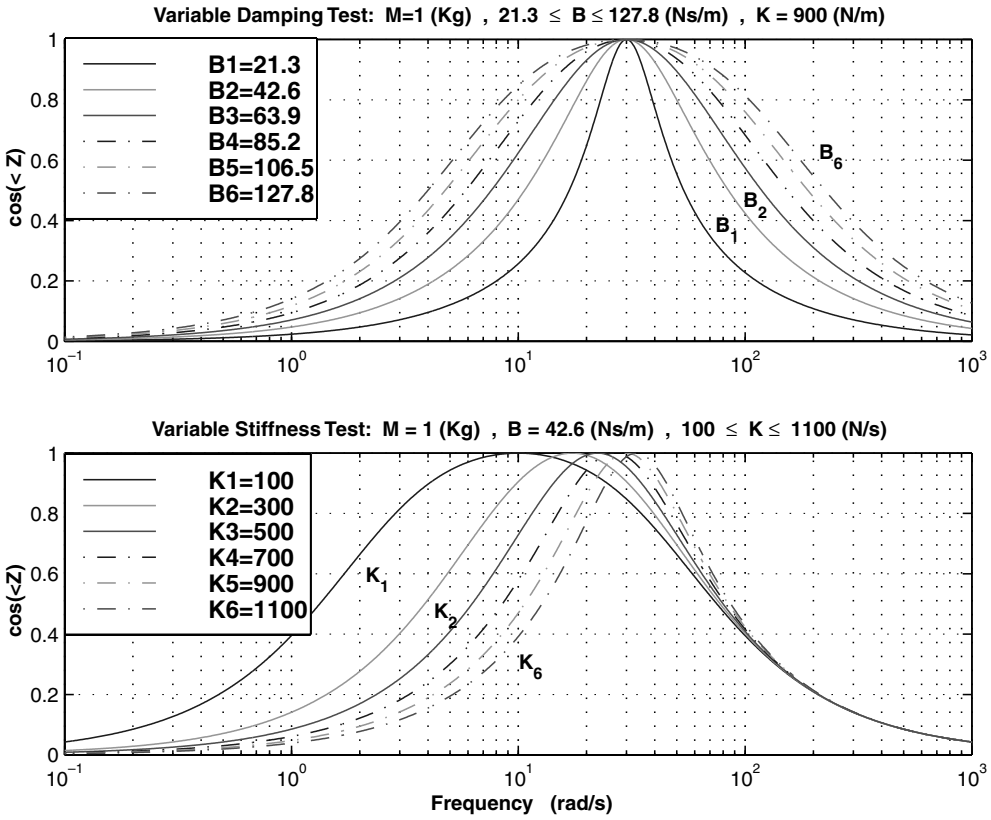

Fig. 3. Study of the effect of damping B and stiffness K on $\cos(\angle Z)$, where $Z := Ms + B + \frac{K}{s}$ is the impedance model of a linear-time-invariant mass-damper-spring system.

there has to be a minimum amount of damping at the master side. The effect of local master force feedback and slave position feedback on absolute stability is not as significant as the effect of local master position and slave force feedback. This makes intuitive sense as the master and slave are only transmitting position and force, respectively. Finally, master damping has a considerably stronger effect on stability than slave damping.

Using the hybrid parameters in (35), Z_{tomin} and $Z_{towidth}$ are derived as

$$Z_{tomin} = \frac{Z_{cm}}{1 + C_6}, \quad Z_{towidth} = \frac{C_1 C_2 e^{-2sT_d}}{(1 + C_5)(1 + C_6)}. \quad (38)$$

Similar to the P-P architecture, an increase in the force feedforward control parameters C_1 and C_2 improves transparency bandwidth. On the other hand, higher local force feedback parameters C_5 and C_6 lead to lower Z_{tomin} and $Z_{towidth}$. A decrease in master local position feedback C_m enhances performance in free motion at the cost of degraded stability robustness.

If the control law (26) is used to achieve the conventional F-P architecture (i.e., $C_1 = Z_{cs}$ and $C_2 = 1 + C_6$) (Lawrence 1993), then η_{fp} in (37) further simplifies to

$$\eta_{fp}(\omega) = \cos(\angle e^{-j2\omega T_d}) + 2\frac{1 + C_5}{1 + C_6}\Re\{Z_{cm}\}\Re\{\frac{1}{Z_{cs}}.\} \quad (39)$$

Comparing (37) and (39), one can see that the stability parameter has been modified such that it is significantly dependent not only on the local master position and slave force feedback but also on the local master force and slave position feedback. For example, higher slave damping may now destabilize the system as $\Re\{\frac{1}{Z_{cs}}\}$ becomes smaller, as shown in Figure 4. In this case, to guarantee stability for any passive operator and environment, $\frac{1+C_5}{1+C_6}\Re\{Z_{cm}\}\Re\{\frac{1}{Z_{cs}}\} \geq 1$ has to hold. This condition is implementable only at midrange frequencies as $\Re\{\frac{1}{Z_{cs}}\}$ vanishes at low and high frequencies. If the time delay is insignificant, then the system is always absolutely stable as $\eta_{fp} \geq 1, \forall\omega \geq 0$. However, in terms of performance, Z_{tomin} does not go to zero and $Z_{towidth}$ does not become infinitely wide, as observed for P-P in Section 5.1.1 and for F-F in Appendix C.

5.1.3. Discussion

By comparing the stability parameters in (32), (37), (50), and (55) and the performance measures in (33), (38), (51), and

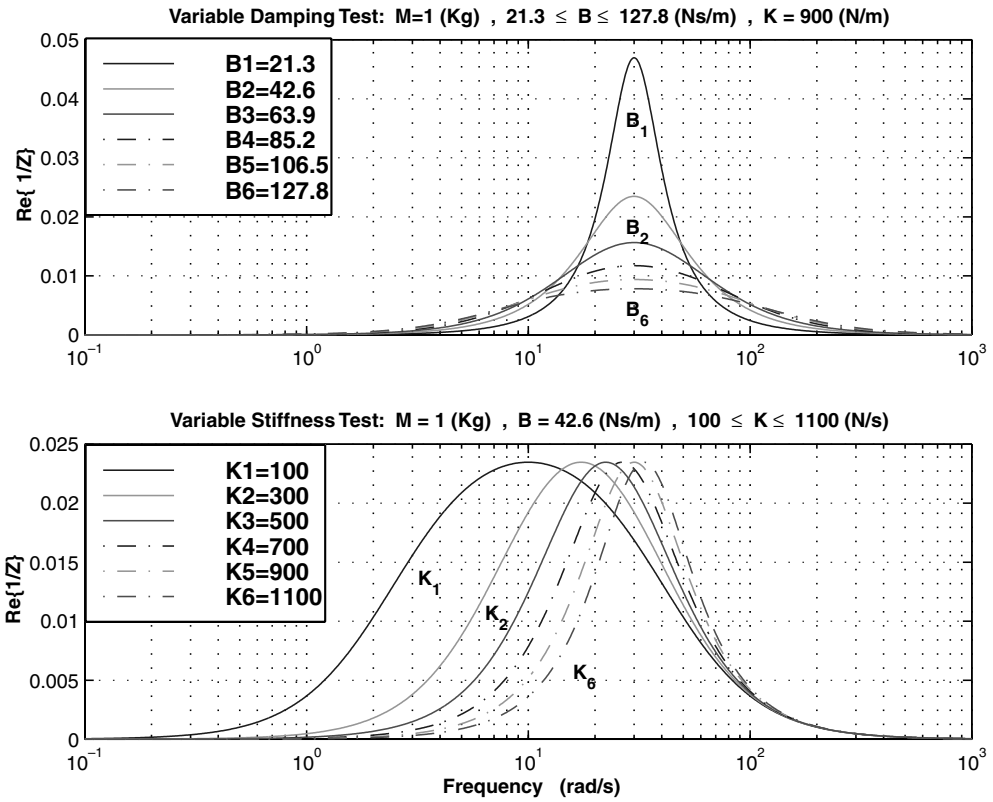

Fig. 4. Effect of damping B and stiffness K on $\Re\{\frac{1}{Z}\}$, where $Z := Ms + B + \frac{K}{s}$ is the impedance model of a linear-time-invariant mass-damper-spring system.

(56), one may conclude the following for any two-channel control architecture:

- Stability robustness is enhanced if the feedforward control parameters are lowered. This is at the cost of smaller dynamic range and/or higher minimum of the transmitted impedance, implying a clear trade-off between stability and performance.

- Regardless of the feedforward control parameters, if the measured force/position signal is sent to the remote manipulator, the local force/velocity feedback at the sender side has more significant influence on the system absolute stability than the local position/force feedback (Fig. 5).

- Performance-wise, an increase in local force feedback parameters attenuates both Z_{tomin} and $Z_{towidth}$. In addition, an increase in local position feedback parameters increases Z_{tomin}.

Based on stability considerations, Table 3 recommends a control architecture (second column) for a particular type of teleoperation system indicated in the first column. The third column indicates two local control parameters that have a significant effect on system stability robustness when the recommended architecture is used. The last column indicates the other two local control parameters that may be used to tune the performance with minimal effect on absolute stability. Note that the control parameters listed in the third column can also be used to tune the performance at the expense of overall system stability robustness. For example, if the master and slave are admittance devices, a P-P control architecture is likely to provide higher stability robustness than other control architectures. In that case, the master and slave local position control parameters have more influence on system absolute stability, whereas local force control parameters can be employed to achieve better performance without compromising absolute stability. However, by comparing the stability parameters in (34), (39), (52), and (57), one observes that the above recommendations are no longer valid if the feedforward parameters are functions of the master and slave dynamics as well as their local control parameters. For example, by employing the transparency-optimized control law (26) in different two-channel architectures, the stability parameters are modified such that the effect of the local force and position feedback on stability robustness changes drastically.

Table 3. General Guideline on Choosing a Control Architecture for a Particular Type of Teleoperation System Based on Stability Considerations

Hardware Master - Slave	Recommended Architecture	Local Feedback	
		Stability	Performance
Admittance - admittance	Position - position	Master position Slave position	Master force Slave force
Admittance - impedance	Force - position	Master position Slave force	Master force Slave position
Impedance - admittance	Position - force	Master force Slave position	Master position Slave force
Impedance - impedance	Force - force	Master force Slave force	Master position Slave position

5.1.4. Simulation Results

In this subsection, a numerical study is employed to explore the stability robustness and performance of F-F, P-P, F-P, and P-F controllers when applied to an impedance-admittance type of teleoperation system. Dynamic simulations using Matlab Simulink are also used to further verify the benefits of the parameter changes suggested for the proposed controllers.

The teleoperation system is assumed to be composed of an impedance-type master with mass model $M_m = 0.7$ Kg, $Z_m = 0.7\ s$ and an admittance-type slave with dynamic model $Y_s = \frac{1}{50s+800+\frac{20{,}000}{s}}$. According to (28), Y_s can be generated by closing a tight position control loop $C_s' V_e = (800 + \frac{20{,}000}{s}) V_e$ around a slave with the impedance mass model $M_s = 50$ Kg, $Z_s = 50\ s$. The manipulators are locally controlled by position compensators $C_m = 29.4 + \frac{630}{s}$ and $C_s = 1300 + \frac{25{,}000}{s}$. The communication delay is assumed to be 100 ms. Considering unity force feedforward scaling $C_2 = C_3 = 1$ and no use of acceleration, the transparency-optimized control parameters are derived from (26) according to $C_1 = C_s + C_s' = 2100 + \frac{45{,}000}{s}$, $C_4 = -C_m = -(29.4 + \frac{630}{s})$, $C_5 = 1 - C_3 = 0$, and $C_6 = 1 - C_2 = 0$.

As seen from Figure 6a, P-F is the only architecture with a stability parameter larger than unity for all frequencies. This verifies the choice of control architecture recommended for the impedance-admittance type of teleoperation system in Table 3. On the other hand, the dual architecture F-P is the least robust as $\eta_{fp} < 1$ for all frequencies. The P-P controller is the second most robust controller, with $\eta_{pp} \leq 1$ only for $4 < \omega < 35$ rad/s. As for performance, from Figures 6b and 6c, P-P and F-P provide the best performance in free space and hard contact with the lowest Z_{tomin} and the highest $Z_{towidth}$, respectively. By contrast, the P-F controller does not show good performance in either free space or in contact.

To better understand the behavior of the above controllers, dynamic simulations are conducted in which the system is triggered by the exogenous input force, as illustrated in Figure 7. Here, $F_h^\star$ is composed of three frequencies 2.3, 6.1 , and 20.9 rad/s. The slave is assumed to either move in free

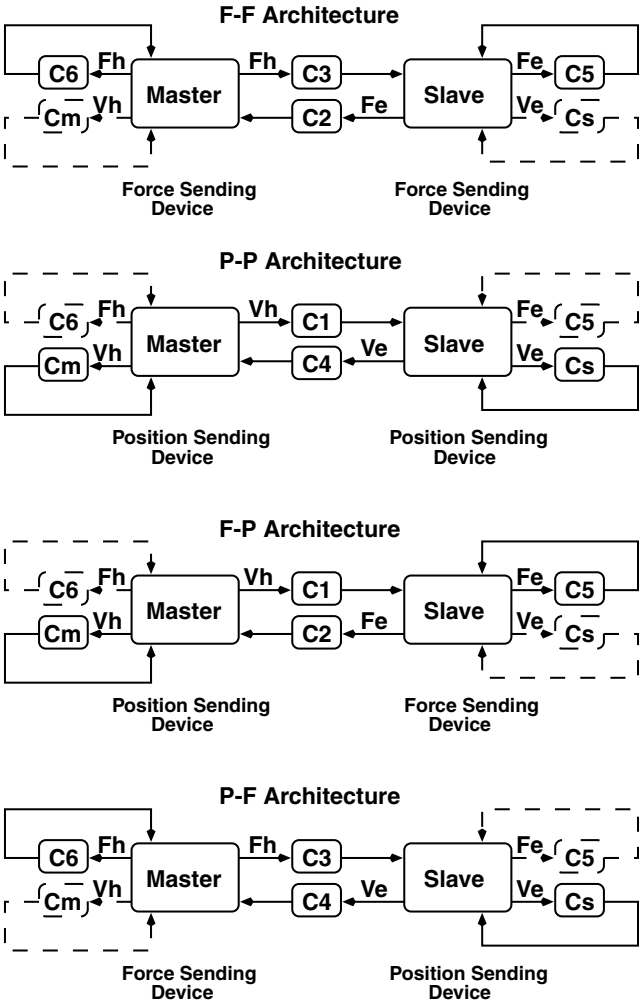

Fig. 5. Control signal flow diagram for the two-channel control architectures. The control paths that have a more significant effect on the system stability robustness are shown with solid lines, and those that have a less significant effect are shown with dashed lines. F-F = force-force, P-P = position-position, F-P = force-position, P-F = position-force.

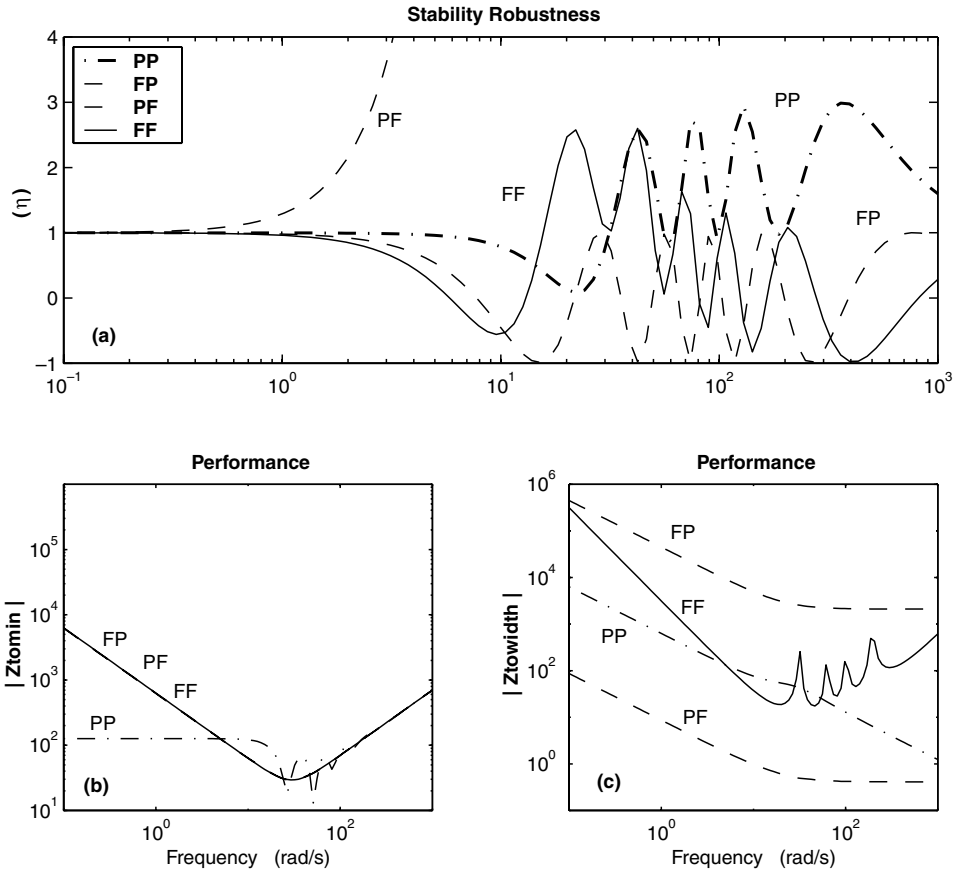

Fig. 6. Stability robustness and performance evaluation and comparison for two-channel control architectures with T_d = 100 ms. P-P = position-position, F-P = force-position, P-F = position-force, F-F = force-force.

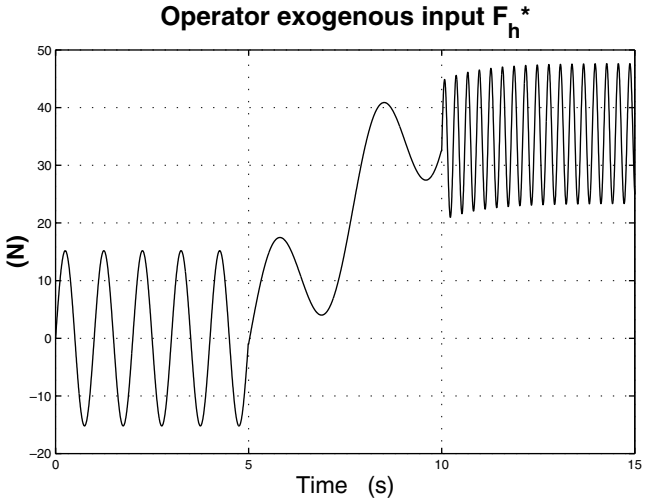

Fig. 7. Operator exogenous input force.

motion $K_e = 0$ or operate on a hard environment with stiffness $K_e = 10^5$ N/m. Figures 8 and 9 show the master and slave performance for both environments.

As seen in Figures 8c and 8d and expected from Figure 6b, the operator feels the lowest impedance in free motion with the P-P controller. However, the operator feels a same higher impedance with other controllers as both the master position and force profiles are almost the same for F-F, F-P, and P-F controllers. The only difference is that the F-P controller provides better position tracking or kinematic correspondence as $|h_{21}| = 1$.

As the environment stiffness increases from zero, the F-P controller becomes unstable for $K_e \geq 2500$ N/m. This may be considered as an indication of lower stability robustness for the F-P architecture, as suggested in Figure 6a. The F-F controller becomes unstable for $K_e \geq 3 \times 10^5$ N/m, and P-P and P-F are stable for a much wider range of environment stiffness. Although potential instability does not imply instability, in this experiment and in the following experiments a general correspondence between the stability parameter and the environment stiffness level above which instability occurs is observed. Simulation results with hard environment $K_e = 10^5$ (N/m) are reported in Figure 9. These results point

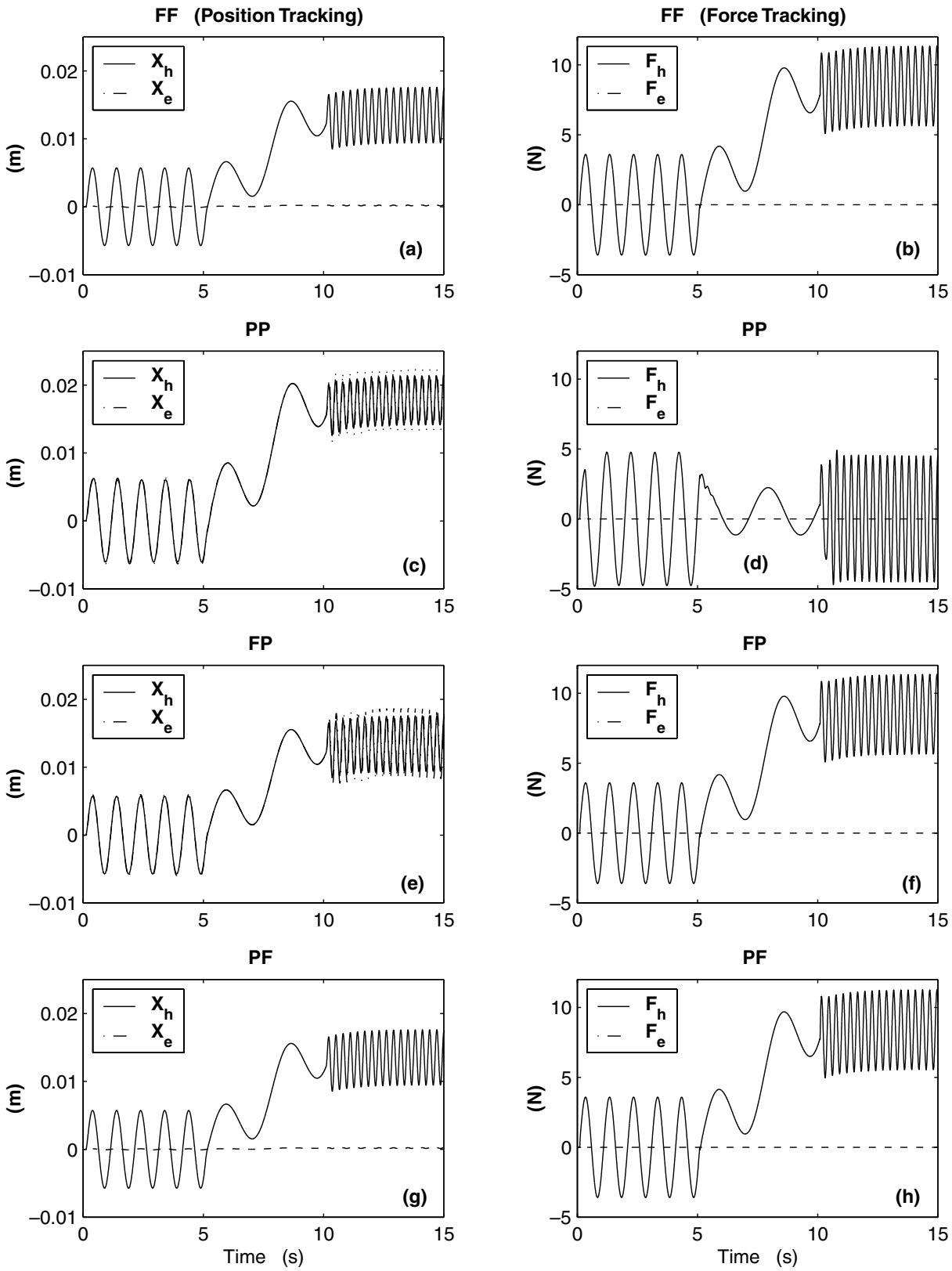

Fig. 8. Position and force tracking performance for two-channel controllers operating in free motion ($K_e = 0$). F-F = force-force; P-P = position-position; F-P = force-position; P-F = position-force.

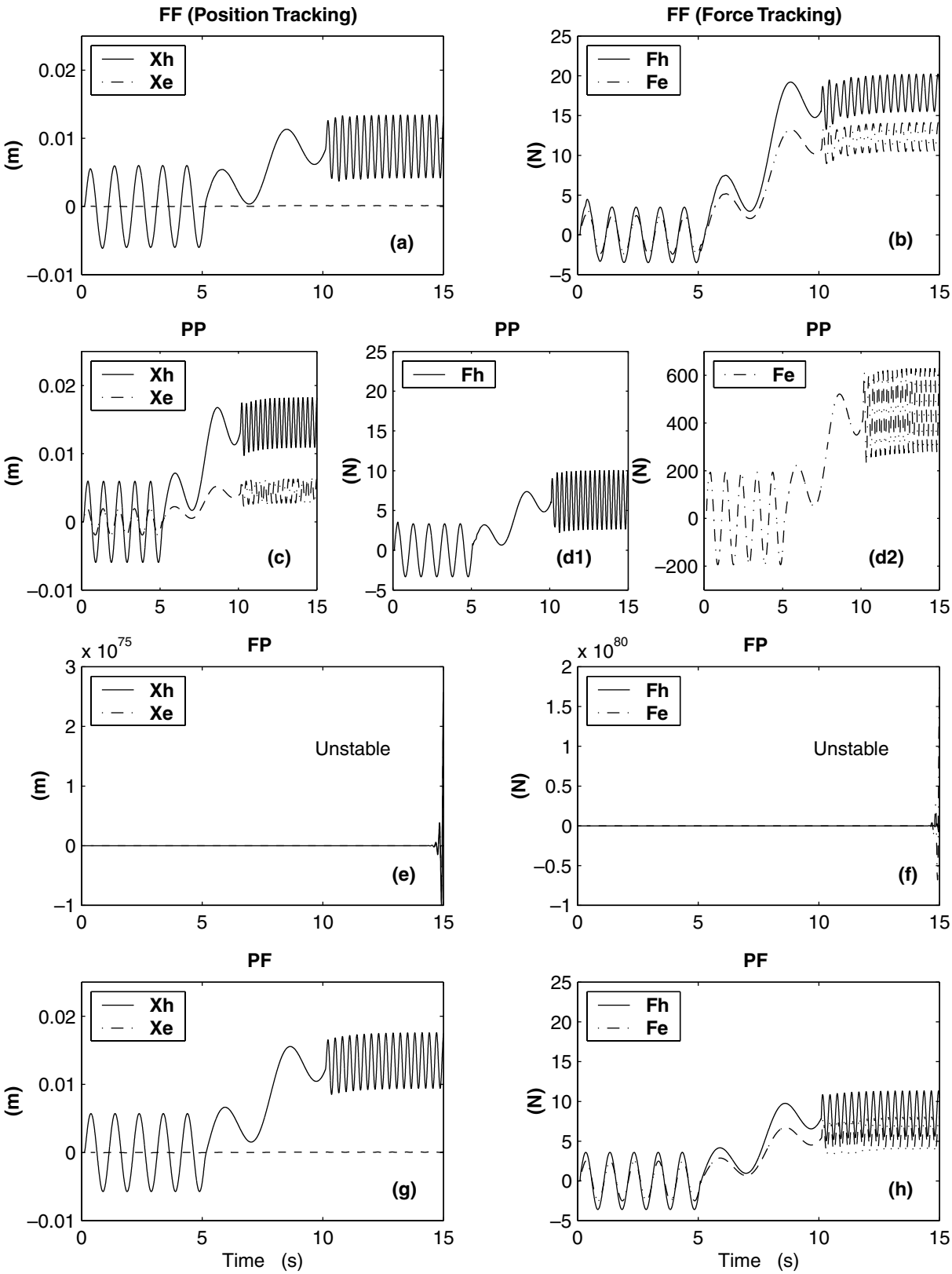

Fig. 9. Position and force tracking performance for two-channel controllers operating in contact ($K_e = 10^5$ N/m). The force-position (F-P) controller is unstable for $K_e \geq 2500$ N/m. F-F = force-force, P-P = position-position, P-F = position-force.

at higher transmitted impedance to the operator by the F-F architecture in comparison to other stable architectures P-P and P-F. As expected, the P-P controller does not provide good contact force control and the P-F and F-F architectures do not provide good position control.

5.2. Suggestions for Stability/Performance Improvements

Based on the analytical results presented in Section 5.1.3, changes to some of the local position and force control parameters are suggested to improve stability and/or performance of the above controllers.

Because the recommended P-F controller is quite robust, changes to the control parameters should be directed toward better transparency performance. As suggested in Table 3, the master local position and the slave local force feedback parameters C_m and C_5 can be adjusted for better performance with minimal degradation in absolute stability. Because only C_m changes $Z_{towidth}$, more damping and stiffness is injected with the new $C_m = 336 + \frac{10080}{s}$. In addition, because of the significant stability robustness, some degradation in the stability robustness may be acceptable. Toward this end, the master local force control parameter C_6, which has significant effect on $Z_{towidth}$, is also modified to $C_6 = -0.67$ for a higher impedance dynamic range. Therefore, to enhance performance, the master has to be transformed to an admittance device. As shown in Figures 10a, 10b, and 10c, the modified P-F controller has a wider $Z_{towidth}$ and yet is still stably robust. Comparing Figures 8g and 8h and Figures 10d and 10e, one realizes that although in free motion ($K_e = 0$), the system is quite stiffer, kinematic correspondence improves significantly. In hard contact ($K_e = 10^5$), both the transmitted impedance and the position and force tracking performance are enhanced significantly (see Figs. 10b, 10c, 10f, and 10g and Figs. 9g and 9h).

As for the P-P controller, which is the second most robust controller, increasing C_m pushes the stability parameter above the unity line, as shown in Figure 11a. Note that as mentioned before, this is equivalent to having an admittance master for which a P-P architecture is recommended in Table 3. An increase in C_m and a decrease in C_6 improves performance by increasing $Z_{tomax} = Z_{tomin} + Z_{towidth} = \frac{Z_{cm}}{1+C_6}$. This improvement in performance is easily observable from comparing the force and position responses in Figures 11f and 11g with those in Figures 9c, 9d-1, and 9d-2. In this case, a higher level of stiffness is transferred to the operator and better position and force tracking is obtained. The drawback is the degradation of transparency in free motion as Z_{tomin} increases. This can also be seen from dynamic simulation results in Figures 11d and 11e, where the hand position/force has decreased/increased significantly. Note that with the above modifications in the master local position and force feedback parameters, the stability robustness, Z_{tomin} and $Z_{towidth}$, of both the P-F and P-P controllers is quite similar with what can be observed from Figures 10a, 10b, and 10c and Figures 11a, 11b, and 11c. In the same way, the position and force responses are the same in Figures 10d, 10e, 10f, and 10g and Figures 11d, 11e, 11f, and 11g.

Because the F-P controller provided the best performance if stable as seen from Figures 6b and 6c and Figures 8e and 8f, one may want to change the local control parameters to increase stability robustness. Toward this end, from (37), one may modify both C_m and C_5 to $336 + \frac{10080}{s}$ and 5 at the cost of an increase in Z_{tomin} and $Z_{towidth}$. As can be seen from Figure 12a, although improved, the stability parameter still remains under the unity level for a wide range of frequencies. This is easily observable from the dynamic simulation results in Figure 12 as the F-P controller remains unstable for $K_e = 10^5$ N/m but is now stable for $K_e \leq 30,000$ N/m instead of 3000 N/m. Therefore, it seems that due to stability considerations, the F-P controller is not a suitable control architecture for the impedance-admittance system considered in this example.

5.3. Four-Channel Control Architecture

In this control architecture, each manipulator sends out both position and force measurements. Therefore, according to the observations made from the analysis for two-channel architectures in Section 5.1, one may conjecture that (i) both local force and position feedback are essential factors in the absolute stability of the system and (ii) by increasing these controls, stability robustness can be guaranteed. Although the former sounds reasonable, in the latter, force and position feedback act in opposite ways, in the sense that one softens and the other stiffens the sender device. Therefore, only one type of control at a time has to be significant depending on the type of the environment to which the sender device is connected. More specifically, when a device is in contact with a hard environment, contact force is the dominant signal for transmission and local force/position control has to be amplified/attenuated. In a dual manner, when a device is in free motion or in contact with a soft environment, position or velocity is the dominant signal for transmission and local position/force control has to be amplified/attenuated. As a result, regardless of the feedforward parameters, there should be a balance between the local position and force feedback levels. This balance can be realized by an adaptive mechanism that automatically detects the contact type and tunes the local feedback parameters accordingly. This strategy has been implemented in a bilateral matched-impedance controller by adjusting the master and slave dynamics based on the environment contact force to velocity ratio (Salcudean et al. 1999).

Figures 13a, 13b, and 13c show the stability parameter, Z_{tomin} and $Z_{towidth}$, of the 4C controller with the original transparency-optimized parameters used in Section 5.1.4. As mentioned in Section 5.1.3, by applying the transparency-optimized law, the feedforward controls counteract the stabilizing effects of local feedback controls. As is seen from

(Continued on page 439)

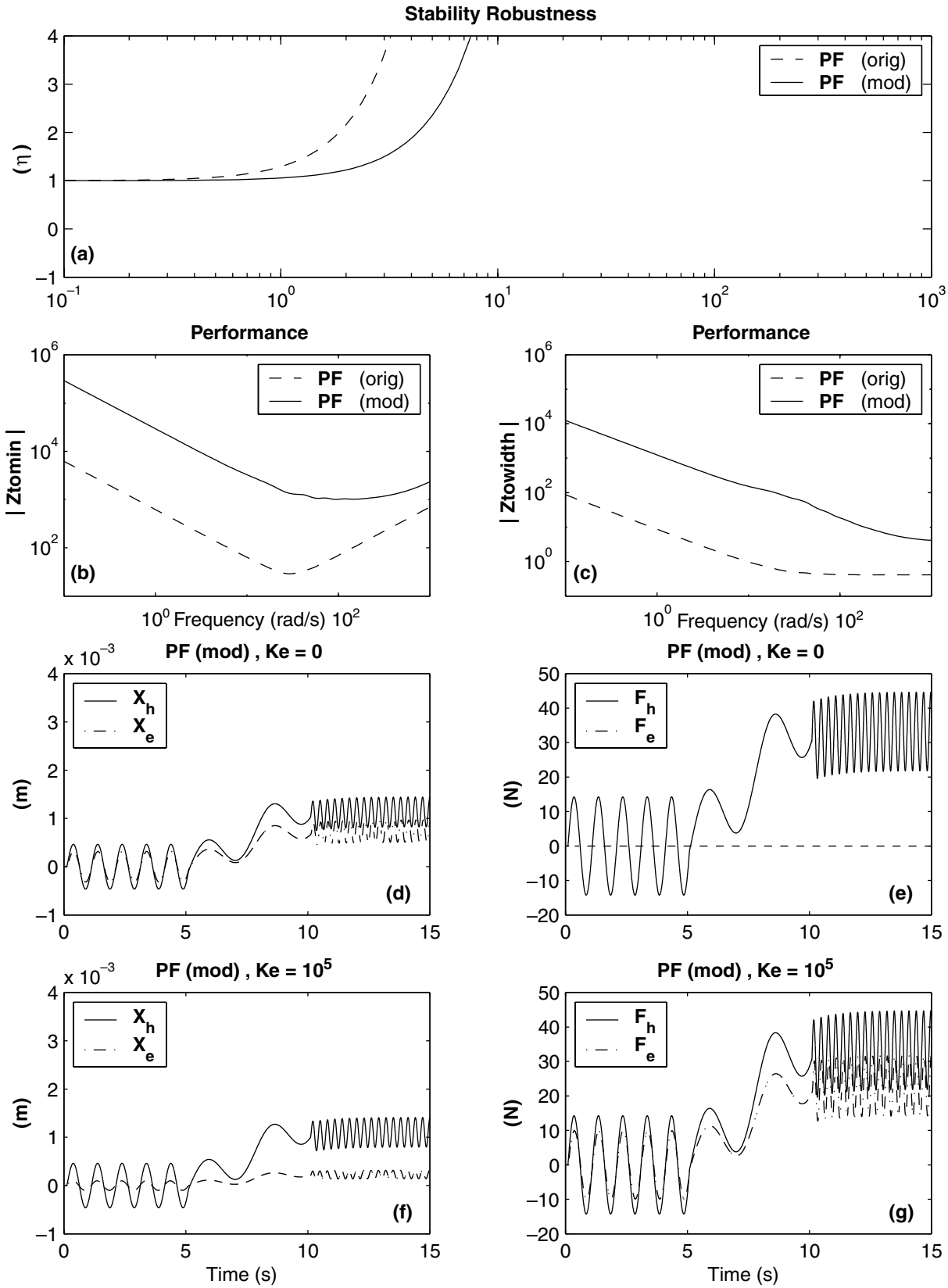

Fig. 10. Stability robustness and performance comparison of the position-force (P-F) controller with original and new master control parameters (a, b, c). The position and force responses with new parameters for free motion and in contact ($K_e = 10^5$ N/m) operations are illustrated in (d, e, f, g).

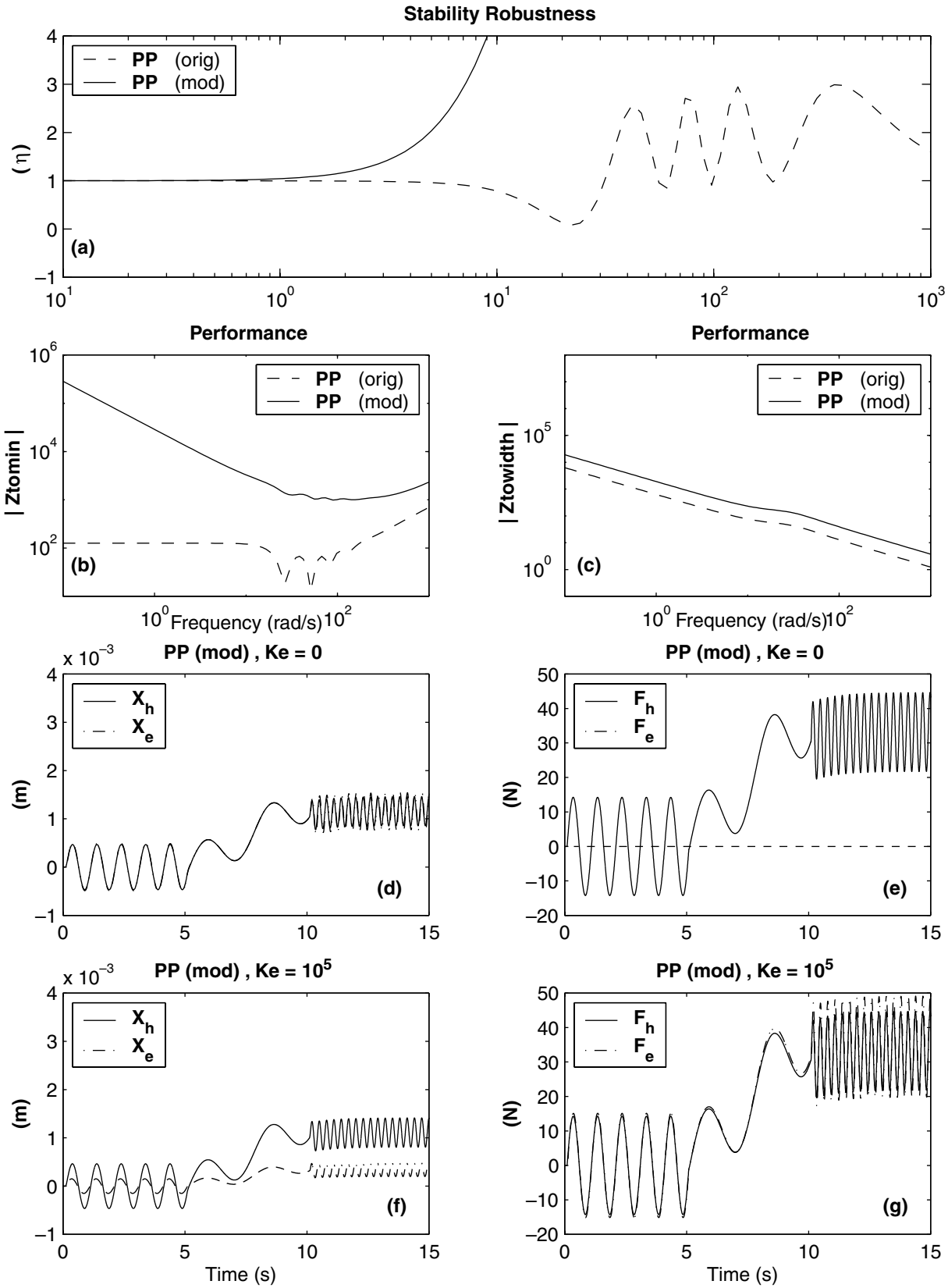

Fig. 11. Stability robustness and performance comparison of the position-position (P-P) controller with original and new master control parameters (a, b, c). The position and force responses with new parameters for free motion and in contact ($K_e = 10^5$ N/m) operations are illustrated in (d, e, f, g).

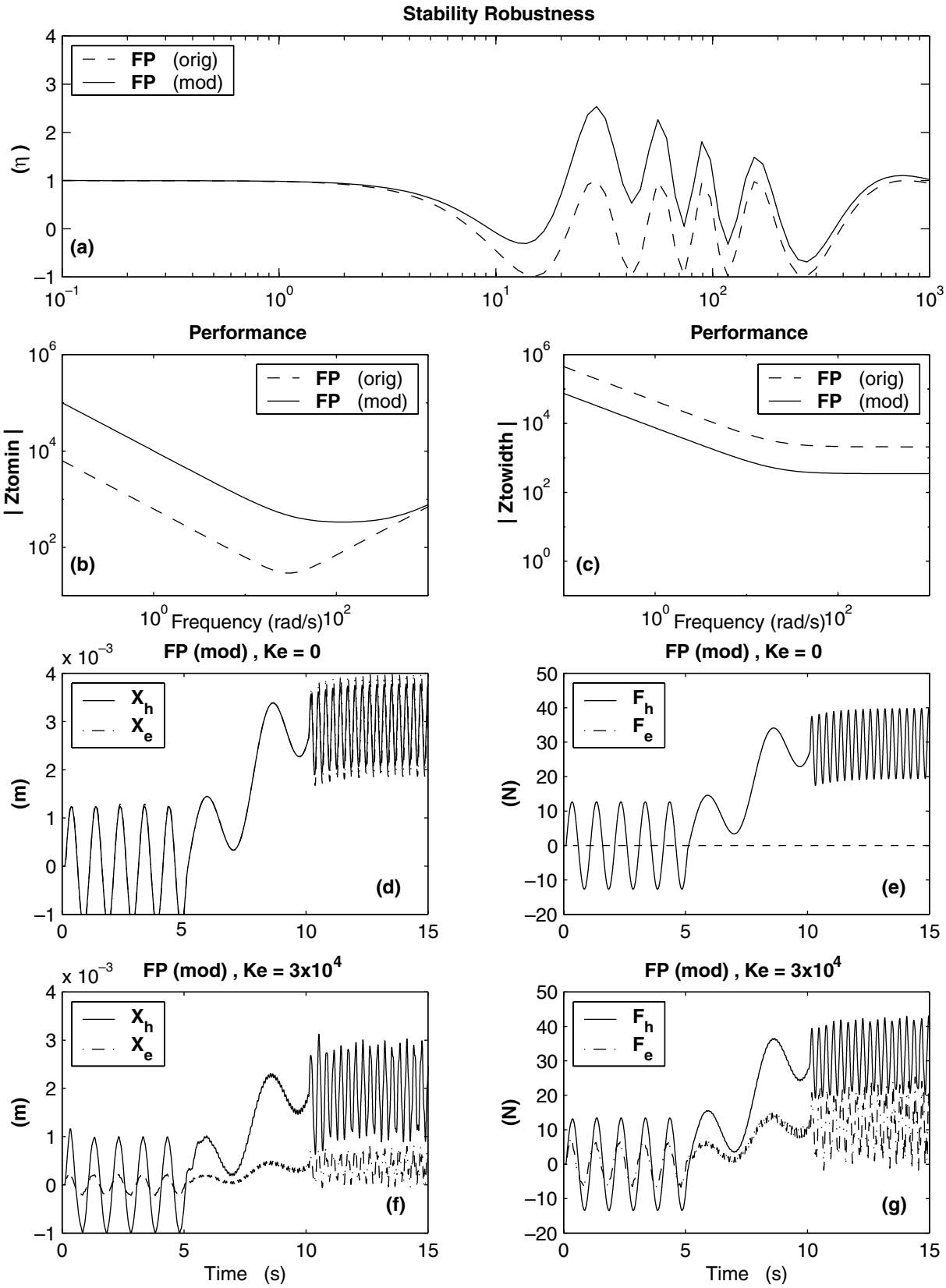

Fig. 12. Stability robustness and performance comparison of the force-position (F-P) controller with original and new master control parameters (a, b, c). The position and force responses with new parameters for free motion and in contact operations ($K_e = 30,000$ N/m) are illustrated in (d, e, f, g). The System is still unstable for $K_e = 10^5$ N/m.

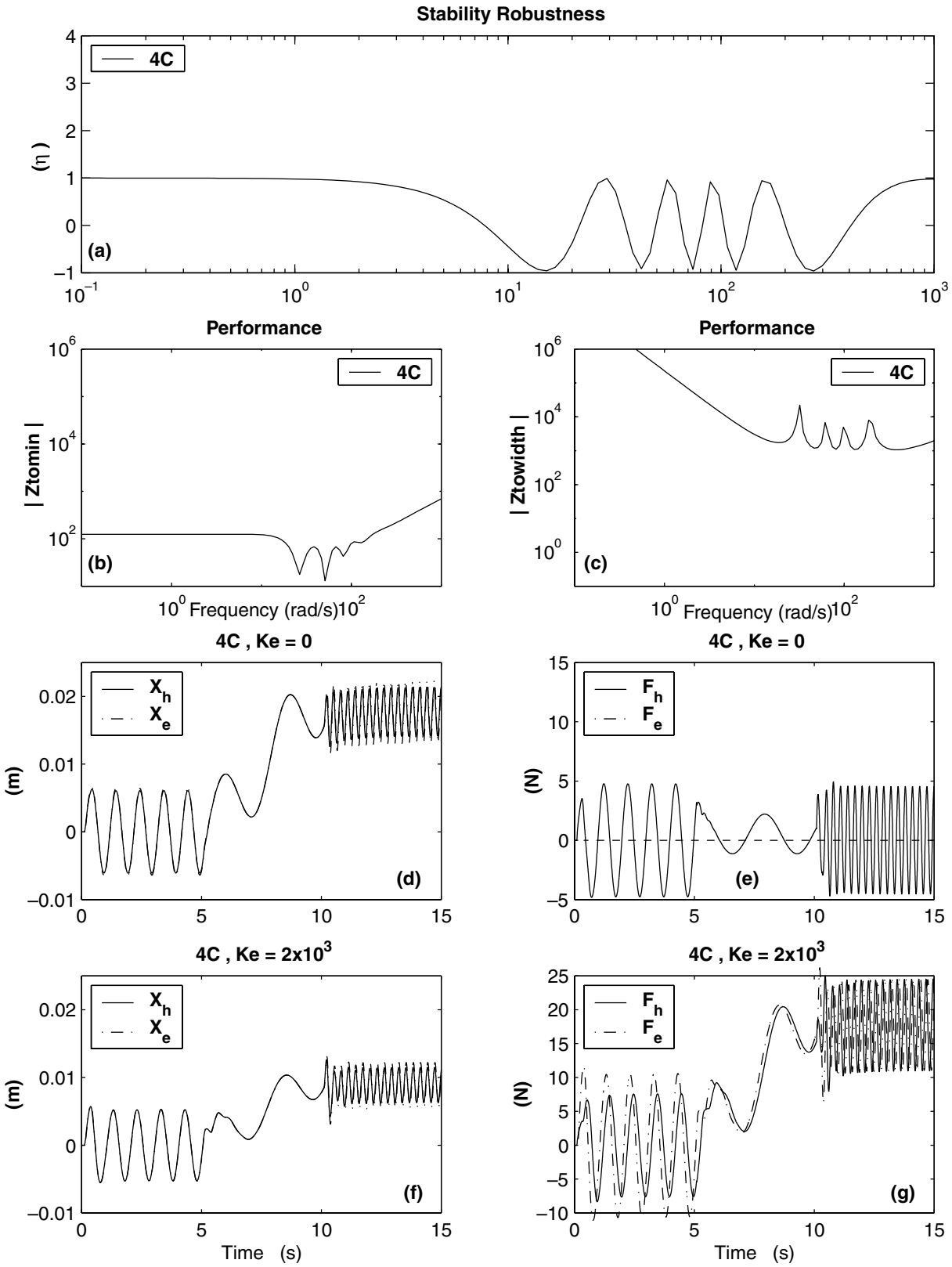

Fig. 13. Stability robustness and performance analysis of the four-channel (4C) controller with original control parameters (a, b, c). The position and force responses for free motion and in contact ($K_e = 2000$ N/m) operations are illustrated in (d, e, f, g). The system is unstable for $K_e = 10^5$ N/m.

Figure 8a and Figure 13a, the transparency-optimized law that is based on the cancellation of the master and slave dynamics seriously jeopardizes stability robustness in most of the control architectures. This is especially noticeable in the case of the F-P and the four-channel control architectures where η is upper bounded by 1. This may make sense as the four-channel controller is unstable for $K_e > 2000$ N/m. Simulation with other types of master and slave manipulators that have not been reported in this paper have resulted in $\eta_{4C} < 1$ for all frequencies. In return, the 4C architecture offers transmitted impedances to the operator with the lowest minimum and the widest bandwidth. This can be observed from Figures 13b and 13c and Figures 8b and 8c, as well as from the position and force responses in Figures 13d, 13e, 13f, and 13g. It can be concluded that the transparency-optimized control law (26) makes the biggest sacrifice of stability for performance when applied to the four-channel control architecture. However, one should note that it is always possible to obtain better stability robustness at the cost of poorer performance by eliminating two data transmission channels, that is, implementing one of the two-channel control architectures.

6. Conclusions

In this paper, the interpretation of the four-channel control architecture based on assumed impedance models of the master and slave was extended to teleoperation systems with admittance master and/or slave.

Conditions on the control parameters leading to perfect transparency when transmission delay is negligible were also derived. The new formalisms can also be used in the design and analysis of teleoperation systems that do not have an impedance model.

Although four-channel control architectures can provide stable perfectly transparent systems in theory, stability and performance for these systems are compromised due to the communication-channel delay as well as the operator and environment dynamic uncertainties. In the second part of this work, the stability and performance robustness of two-channel and four-channel control architectures were analyzed using Llewellyn's absolute stability criterion as well as the minimum (Z_{tomin}) and dynamic range ($Z_{towidth}$) of the transmitted impedance to the operator. These analysis tools can provide clear insight into the significance of the control parameters on stability robustness and performance. It has been shown that by proper selection of the MSN parameters, it is possible to analytically study robustness in two-channel architectures, whereas for more complicated schemes, such as four-channel architectures, numerical evaluations can be employed.

The analysis of two-channel architectures has pointed at the trade-offs between stability and performance in terms of the control parameters, especially the force feedforward parameters. In particular, stability robustness is enhanced at the cost of smaller $Z_{towidth}$ if the feedforward control parameters are lowered. On the other hand, the effect of local control parameters depends on the control architecture and the feedforward control parameters chosen. The analysis has shown that regardless of the feedforward control parameters, the force-force, position-position, force-position, and position-force architectures are likely to provide higher stability robustness to the impedance-impedance, admittance-admittance, admittance-impedance, and impedance-admittance types of teleoperation systems, respectively. Performance-wise, an increase in local force feedback parameters attenuates both Z_{tomin} and $Z_{towidth}$ and an increase in local position feedback parameters increases Z_{tomin}. Some of the above conclusions were validated by dynamic simulation of an impedance-admittance type of teleoperation control system. To increase stability robustness in four-channel control architectures, the above analysis also suggested the adaptation of the master and slave dynamics based on the operator and environment contact types.

The above assertions may change if the feedforward control parameters are functions of the master and slave dynamics and their local control parameters. This is clearly visible in the conventional two-channel control architectures. As an example, it has been observed from the numerical analysis results that the transparency-optimized control law (26) severely degrades stability robustness of the architectures with two channels and especially four channels of data transmission. Instead, the four-channel control architecture provides the best transparency performance.

Appendix A: Effect of Operator and Environment Impedance on Absolute Stability

Consider a teleoperation system with master-slave two-port network $\mathcal{N}$ connected to an operator and an environment as shown in Figure 14. The operator and environment impedances are split into nominal passive impedances Z_h and Z_e with infinite dynamic range, and shunt passive impedances $\bar{Z}_h$ and $\bar{Z}_e$ representing the operator and the environment maximum impedances. Because the dynamic range of the operator and environment impedances is finite, the absolute stability of $\mathcal{N}$ that assumes infinite dynamic range for the operator and environment may provide a rather conservative stability robustness condition set. A more relaxed set of conditions may be found by examining the absolute stability of the new two-port network $\mathcal{N}'$ created by absorbing $\bar{Z}_h$ and $\bar{Z}_e$ into $\mathcal{N}$. In this case, Z_h and Z_e that are connected to $\mathcal{N}'$ have infinite dynamic range. Therefore, Llewellyn's absolute stability criterion can easily be applied as follows:

$$\eta'_{\mathcal{H}} = -\cos(\angle h'_{12}h'_{21}) + 2\frac{\Re\{h'_{11}\}\Re\{h'_{22}\}}{|h'_{12}h'_{21}|} \quad (40)$$

$$\Re\{h'_{11}\} \geq 0, \quad (41)$$

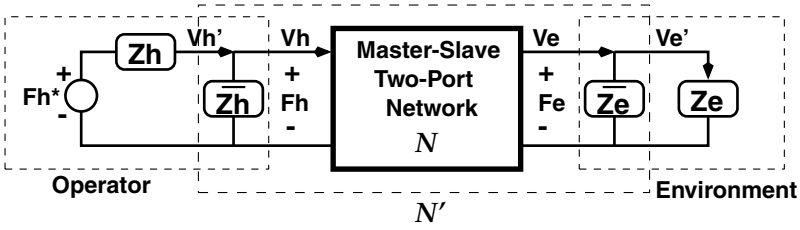

Fig. 14. Block diagram of a teleoperation system when the operator and environment maximum impedance values are bounded by $\bar{Z}_h$ and $\bar{Z}_e$, respectively.

where $\eta'_{\mathcal{H}}$ is the stability parameter associated with $\mathcal{N}'$ and $h'_{11}, h'_{12}, h'_{21}$, and h'_{22} are the hybrid parameters of $\mathcal{N}'$ defined as

$$\begin{bmatrix} F_h \\ -V'_e \end{bmatrix} := \begin{bmatrix} h'_{11} & h'_{12} \\ h'_{21} & h'_{22} \end{bmatrix} \begin{bmatrix} V'_h \\ F_e \end{bmatrix}. \tag{42}$$

After substituting for the through variables V_h and V_e from

$$V_h = V'_h - \frac{F_h}{\bar{Z}_h} \quad , \quad V_e = V'_e + \frac{F_e}{\bar{Z}_e} \tag{43}$$

into (5) and comparing the resulting dynamics with (42), the new hybrid matrix $\mathcal{H}'$ can be expressed in terms of the original hybrid parameters as

$$H' = \begin{bmatrix} \frac{h_{11}\bar{Z}_h}{\bar{Z}_h + h_{11}} & \frac{h_{12}\bar{Z}_h}{\bar{Z}_h + h_{11}} \\ \frac{h_{21}\bar{Z}_h}{\bar{Z}_h + h_{11}} & h_{22} - \frac{h_{12}h_{21}}{\bar{Z}_h + h_{11}} + \frac{1}{\bar{Z}_e} \end{bmatrix}. \tag{44}$$

If the performance of the teleoperator is close to transparent, then h_{11} is small such that $h_{11} \ll \bar{Z}_h$ and $\mathcal{H}'$ can be approximated by

$$H' := \begin{bmatrix} h'_{11} & h'_{12} \\ h'_{21} & h'_{22} \end{bmatrix} \approx \begin{bmatrix} h_{11} & h_{12} \\ h_{21} & h_{22} - \frac{h_{12}h_{21}}{\bar{Z}_h} + \frac{1}{\bar{Z}_e} \end{bmatrix}. \tag{45}$$

Because $\Re\{h_{22} + \frac{-h_{12}h_{21}}{\bar{Z}_h} + \frac{1}{\bar{Z}_e}\} = \Re\{h_{22}\} + \Re\{\frac{-h_{12}h_{21}}{\bar{Z}_h}\} + \Re\{\frac{1}{\bar{Z}_e}\}$, stability parameter $\eta'_{\mathcal{H}}$ in (40) can now be expanded and expressed in terms of the original hybrid parameters as

$$\begin{aligned} \eta'_{\mathcal{H}} = & -\cos(\angle h_{12}h_{21}) + 2\frac{\Re\{h_{11}\}\Re\{h_{22}\}}{|h_{12}h_{21}|} \\ & + 2\frac{\Re\{h_{11}\}\Re\{\frac{-h_{12}h_{21}}{\bar{Z}_h}\}}{|h_{12}h_{21}|} + 2\frac{\Re\{h_{11}\}\Re\{\frac{1}{\bar{Z}_e}\}}{|h_{12}h_{21}|}. \end{aligned} \tag{46}$$

The first two terms on the right-hand side of (46) constitute $\eta_{\mathcal{H}}$, that is, the stability parameter of $\mathcal{N}$ derived by incorporating h_{11}, h_{12}, h_{21}, and h_{22} in the Llewellyn conditions (8)-(9). Therefore, $\eta'_{\mathcal{H}}$ can be further simplified as

$$\begin{aligned} \eta'_{\mathcal{H}} &= \eta_{\mathcal{H}} + 2\frac{\Re\{h_{11}\}\Re\{\frac{-h_{12}h_{21}}{\bar{Z}_h}\}}{|h_{12}h_{21}|} + 2\frac{\Re\{h_{11}\}\Re\{\frac{1}{\bar{Z}_e}\}}{|h_{12}h_{21}|} \\ &= \eta_{\mathcal{H}} + 2\frac{\Re\{h_{11}\}}{|\bar{Z}_h|}\cos(\angle\frac{-h_{12}h_{21}}{\bar{Z}_h}) \\ &\quad + 2\frac{\Re\{h_{11}\}\Re\{\frac{1}{\bar{Z}_e}\}}{|h_{12}h_{21}|}. \end{aligned} \tag{47}$$

Because $\bar{Z}_h$ and $\bar{Z}_e$ are both assumed to be passive, $-90° < \angle\bar{Z}_h < 90°$ and $\Re\{\frac{1}{\bar{Z}_e}\} > 0$ hold. Considering this and that $\Re\{h_{11}\} \geq 0$ in (8) for $\mathcal{N}$, the following results are concluded from (47):

- The limitation on the *environment* impedance dynamic range adds positive value to the stability parameter $\eta_{\mathcal{H}}$, resulting in a more relaxed absolute stability condition-set.

- If h_{12} and h_{21} are in opposite directions, that is, $\angle h_{12}h_{21} = 180°$, then the limitation on the *operator* impedance dynamic range enhances the system stability robustness by adding positive value to $\eta_{\mathcal{H}}$. In fact, this is the case for transparent teleoperation systems in which $h_{12}h_{21} = -1$. If $\angle h_{12}h_{21} \neq 180°$, then at low or high frequencies stability robustness is degraded as $\cos(\angle\frac{-h_{12}h_{21}}{\bar{Z}_h}) < 0$. The only exception is when $\bar{Z}_h$ holds a strong damping property. In this case, stability robustness still improves as long as $\angle h_{12}h_{21} \geq 90°$.

Appendix B: Four-Channel Controller for Teleoperators with Admittance Master and/or Slave

In this appendix, perfect transparency conditions for teleoperation systems with admittance master and/or slave are summarized in Tables 4, 5, and 6. Note that $Y_{em} := Y_m + E_m^{-1}$ and $Y_{es} := Y_s + E_s^{-1}$.

Table 4. Master-Slave Two-Port Network Parametric Specifications and the Transparency-Optimized Law for Impedance-Admittance Type Teleoperation Systems Controlled by a General Four-Channel Bilateral Controller

Master-slave two-port network hybrid parameters	$h_{11} = \frac{(1+E_5)Z_{cm}+E_3C_4e^{-2sT_d}}{(1+E_5)(1+C_6)-E_1^{-1}C_4e^{-2sT_d}}$ $h_{12} = \frac{C_2(1+E_5)e^{-sT_d}-C_4Y_{es}e^{-sT_d}}{(1+E_5)(1+C_6)-E_1^{-1}C_4e^{-2sT_d}}$ $h_{21} = -\frac{E_3(1+C_6)e^{-sT_d}+E_1^{-1}Z_{cm}e^{-sT_d}}{(1+E_5)(1+C_6)-E_1^{-1}C_4e^{-2sT_d}}$ $h_{22} = \frac{(1+C_6)Y_{es}-E_1^{-1}C_2e^{-2sT_d}}{(1+E_5)(1+C_6)-E_1^{-1}C_4e^{-2sT_d}}$
Transmitted impedance	$Z_{to} = \frac{[(1+E_5)Z_{cm}+E_3C_4e^{-2sT_d}]+[Z_{cm}Y_{es}+C_2E_3e^{-2sT_d}]Z_e}{[(1+E_5)(1+C_6)-E_1^{-1}C_4e^{-2sT_d}]+[(1+C_6)Y_{es}+E_1^{-1}C_2e^{-2sT_d}]Z_e}$
Transparency-optimized control law	$E_1^{-1} = Y_{es},\ C_2 = 1 + C_6,\ E_3 = 1 + E_5,\ C_4 = -Z_{cm},\ (C_2, E_3) \neq (0, 0)$

Table 5. Master-Slave Two-Port Network Parametric Specifications and the Transparency-Optimized Law for Admittance-Impedance Type Teleoperation Systems Controlled by a General Four-Channel Bilateral Controller

Master-slave two-port network hybrid parameters	$h_{11} = \frac{(1+E_6)Z_{cs}-C_1E_2e^{-2sT_d}}{Y_{em}Z_{cs}+E_2C_3e^{-2sT_d}}$ $h_{12} = \frac{E_4^{-1}Z_{cs}e^{-sT_d}+E_2(1+C_5)e^{-sT_d}}{Y_{em}Z_{cs}+E_2C_3e^{-2sT_d}}$ $h_{21} = -\frac{C_3(1+E_6)e^{-sT_d}+C_1Y_{em}e^{-sT_d}}{Y_{em}Z_{cs}+E_2C_3e^{-2sT_d}}$ $h_{22} = \frac{(1+C_5)Y_{em}+C_3E_4^{-1}e^{-2sT_d}}{Y_{em}Z_{cs}+E_2C_3e^{-2sT_d}}$
Transmitted impedance	$Z_{to} = \frac{[(1+E_6)Z_{cs}-C_1E_2e^{-2sT_d}]+[(1+C_5)(1+E_6)-C_1E_4^{-1}e^{-2sT_d}]Z_e}{[Y_{em}Z_{cs}+E_2C_3e^{-2sT_d}]+[(1+C_5)Y_{em}+C_3E_4^{-1}e^{-2sT_d}]Z_e}$
Transparency-optimized control law	$C_1 = Z_{cs},\ E_2 = 1 + E_6,\ C_3 = 1 + C_5,\ E_4^{-1} = -Y_{em},\ (E_2, C_3) \neq (0, 0)$

Table 6. Master-Slave Two-Port Network Parametric Specifications and the Transparency-Optimized Law for Admittance-Admittance Type Teleoperation Systems Controlled by a General Four-Channel Bilateral Controller

Master-slave two-port network hybrid parameters	$h_{11} = \frac{(1+E_5)(1+E_6)-E_2E_3e^{-2sT_d}}{(1+E_5)Y_{em}+E_1^{-1}E_2e^{-2sT_d}}$ $h_{12} = \frac{-E_4^{-1}(1+E_5)e^{-sT_d}+E_2Y_{es}e^{-sT_d}}{(1+E_5)Y_{em}+E_1^{-1}E_2e^{-2sT_d}}$ $h_{21} = \frac{E_1^{-1}(1+E_6)e^{-sT_d}+E_3Y_{em}e^{-sT_d}}{(1+E_5)Y_{em}+E_1^{-1}E_2e^{-2sT_d}}$ $h_{22} = \frac{Y_{em}Y_{es}+E_1^{-1}E_4^{-1}e^{-2sT_d}}{(1+E_5)Y_{em}+E_1^{-1}E_2e^{-2sT_d}}$
Transmitted impedance	$Z_{to} = \frac{[(1+E_5)(1+E_6)-E_2E_3e^{-2sT_d}]+[(1+E_6)Y_{es}+E_3E_4^{-1}e^{-2sT_d}]Z_e}{[(1+E_5)Y_{em}+E_1^{-1}E_2e^{-2sT_d}]+[Y_{em}Y_{es}+E_1^{-1}E_4^{-1}e^{-2sT_d}]Z_e}$
Transparency-optimized control law	$E_1^{-1} = Y_{es},\ E_2 = 1+E_6,\ E_3 = 1+E_5,\ E_4^{-1} = -Y_{em},\ (E_2, E_3) \neq (0,0)$

Appendix C: Analysis of Force-Force and Position-Force Control Architectures

Force-Force Control Architecture

In the force-force (F-F) control architecture, proposed by Kazerooni, Tsay, and Hollerbach (1993), the coordinating force feedforward controls are removed; that is, $C_1 = C_4 = 0$. In this case, it is easiest to analyze stability robustness in terms of the master-slave two-port network admittance parameters

$$y_{11} := \frac{1}{h_{11}} = \frac{1+C_6}{Z_{cm}}, \qquad y_{12} := \frac{h_{12}}{h_{11}} = \frac{-C_2e^{-sT_d}}{Z_{cm}}$$
$$y_{21} := \frac{-h_{12}}{h_{11}} = \frac{-C_3e^{-sT_d}}{Z_{cs}}, \quad y_{22} := \frac{\Delta h}{h_{11}} = \frac{1+C_5}{Z_{cs}}. \quad (48)$$

From (9),

$$\eta_{ff}(\omega) := \eta_{ff1} + \eta_{ff2} = -\cos(\angle\frac{C_2C_3e^{-j2\omega T_d}}{Z_{cm}Z_{cs}}) + 2\frac{\Re\{\frac{1+C_6}{Z_{cm}}\}\Re\{\frac{1+C_5}{Z_{cs}}\}}{|\frac{C_2C_3e^{-j2\omega T_d}}{Z_{cm}Z_{cs}}|} \quad (49)$$
$$= sgn(C_2C_3)[-\cos(\angle Z_{cm}Z_{cs}e^{j2\omega T_d}) + 2\frac{(1+C_5)(1+C_6)}{C_2C_3}\cos(\angle Z_{cm})\cos(\angle Z_{cs})]. \quad (50)$$

The delay-dependent terms are lumped into η_{ff1}. Because $\eta_{ff1} \in [-1, 1]$ and includes $e^{j2\omega T_d}$, the absolute stability of the system can be guaranteed only when $\eta_{ff2} \geq 2$. Because Z_{cm} and Z_{cs} are passive, $-90° < \angle Z_{cm}, \angle Z_{cs} < 90°$ holds, and as a result $\cos(\angle Z_{cm})\cos(\angle Z_{cs}) \in [0, 1]$. Therefore, to guarantee absolute stability for only some range of frequencies, $(1+C_5)(1+C_6) > |C_2C_3|$ must hold, implying higher amount of local force feedback (lower master and slave total impedances) or lower amount of force feedforward. This suggests that in terms of stability robustness, the F-F control architecture is more suitable for an impedance-impedance type of teleoperation system. In addition, Z_{cm} and Z_{cs} and, consequently, the local position control parameters do not have as much effect on absolute stability as do the local force control parameters C_5 and C_6. Because at high frequencies η_{ff1} fluctuates between -1 and 1, and $\cos(\angle Z_{cm})\cos(\angle Z_{cs}) \to 0$, the force control parameters cannot guarantee absolute stability for all frequencies unless the force feedforward parameters C_2 and C_3 are low-pass filters instead of constant gains as assumed in Table 1. In this case, (50) is not valid anymore and (49) has to be used instead. The idea of low-pass filtering the feedforward signals for enhanced stability was discussed in Yoshikawa and Ueda (1996) and Eusebi and Melchiorri (1998).

To study performance, the hybrid parameters are incorporated in (13)-(14) to yield

$$Z_{tomin} = \frac{Z_{cm}}{1+C_6}$$
$$Z_{towidth} = \frac{C_2 C_3 Z_{tomin} e^{-2sT_d}}{(1+C_5)(1+C_6) - C_2 C_3 e^{-2sT_d}}. \quad (51)$$

Similar to the position-position (P-P) and force-position (F-P) cases, an increase in the force feedforward parameters C_2 and C_3 improves performance as stability robustness degrades. On the other hand, increasing local force feedback parameters C_5 and C_6 has a mixed effect on performance as both Z_{tomin} and $Z_{towidth}$ decrease. This indicates that the stability versus performance trade-off is less evident when tuning local force control parameters. Amplification of local position feedback in Z_{cm} increases transparency dynamic range at the cost of poor performance in free motion as the master becomes sluggish. This is due to the fact that $Z_{towidth}$ is proportional to Z_{tomin}.

If the transparency-optimized control law (26) is used to choose the feedforward control parameters according to $C_2 = C_6 + 1$ and $C_3 = C_5 + 1$, then η_{ff} simplifies to

$$\eta_{ff}(\omega) = sgn((1+C_5)(1+C_6))[-\cos(\angle Z_{cm} Z_{cs} e^{j2\omega T_d}) + 2\cos(\angle Z_{cm})\cos(\angle Z_{cs})] \quad (52)$$

and the stability parameter is no longer a function of the force feedback nor a strong function of feedforward parameters C_5, C_6, C_2, and C_3. The only way to slightly improve the stability robustness is through $\cos(\angle Z_{cm})$ and $\cos(\angle Z_{cs})$ by increasing the relative amount of damping in the master and slave dynamics. If the time delay is negligible, by using hybrid parameters it is possible to show that $\eta_{ff} = sgn(\frac{1+C_5}{1+C_6})\cos(\angle \frac{Z_{cm}}{Z_{cs}}) \leq 1, \forall \omega \geq 0$ and $Z_{towidth} \to \infty$, implying a wide range of transmitted impedance at the cost of potential instability. In the same way as in the P-P architecture, η_{ff} is maximized to unity at all frequencies if $\frac{M_m}{M_s} = \frac{B_m}{B_s} = \frac{K_m}{K_s}$ holds.

Position-Force Control Architecture

The position-force (P-F) control architecture has not yet been implemented, except for in haptic simulation applications in Adams and Hannaford (1999), where this architecture was employed to communicate between an admittance-type haptic device and a virtual environment. In this architecture, the direct force feedforward from the slave to the master and the coordinating force feedforward from the master to the slave are removed; that is, $C_1 = C_2 = 0$. The inverse hybrid parameters

$$g_{11} := \frac{h_{22}}{\Delta h} = \frac{1+C_6}{Z_{cm}}, \qquad g_{12} := \frac{-h_{12}}{\Delta h} = \frac{C_4 e^{-sT_d}}{Z_{cm}}$$
$$g_{21} := \frac{-h_{21}}{\Delta h} = \frac{C_3 e^{-sT_d}}{1+C_5}, \quad g_{22} := \frac{h_{11}}{\Delta h} = \frac{Z_{cs}}{1+C_5} \quad (53)$$

can be used to easily evaluate η_{pf} according to

$$\eta_{pf}(\omega) := \eta_{pf1} + \eta_{pf2} = -\cos(\angle \frac{C_3 C_4 e^{-j2\omega T_d}}{(1+C_5)Z_{cm}}) + 2\frac{\Re\{\frac{1+C_6}{Z_{cm}}\}\Re\{\frac{Z_{cs}}{1+C_5}\}}{|\frac{C_3 C_4 e^{-j2\omega T_d}}{(1+C_5)Z_{cm}}|} \quad (54)$$

$$= sgn(1+C_5)[-\cos(\angle \frac{C_3 C_4 e^{-j2\omega T_d}}{Z_{cm}}) + 2\frac{(1+C_6)\Re\{Z_{cs}\}}{|C_3 C_4|}\cos(\angle \frac{1}{Z_{cm}})]. \quad (55)$$

Dual to the F-P architecture, the absolute stability condition (9) is met over a certain range of frequencies in which $\eta_{pf2} \geq 2$, that is, when $(1+C_6)\Re\{Z_{cs}\} \geq sgn(1+C_5)|C_3 C_4|$. This implies that in order to increase stability robustness, slave damping and master local force feedback should be increased (higher slave and lower master impedances) whereas force feedforward parameters should be decreased. This suggests that the P-F architecture is more likely to be stable for the impedance-admittance type of teleoperation system. In addition, there has to be a minimum amount of damping in the slave. To increase stability robustness at high frequencies despite convergence of $\cos(\angle \frac{1}{Z_{cm}})$ to zero, the feedforward control parameter C_3 has to be a low-pass filter instead of a constant as assumed in Table 1. Also from (55), the effect of local slave force and master position feedback on absolute stability is not as significant as the effect of the local slave position and master force feedback. Finally, damping at the slave side has a stronger effect on stability than damping at the master side.

Using the hybrid parameters, $Z_{towidth}$ and $Z_{towidth}$ are derived as

$$Z_{tomin} = \frac{Z_{cm} Z_{cs}}{(1+C_6)Z_{cs} - C_3 C_4 e^{-2sT_d}}$$
$$Z_{towidth} = \frac{-C_3 C_4 Z_{cm} e^{-2sT_d}}{(1+C_6)[(1+C_6)Z_{cs} - C_3 C_4 e^{-2sT_d}]}. \quad (56)$$

As with the other architectures, performance improves as the force feedforward control parameters increase. In addition, higher local force feedback decreases both Z_{tomin} and $Z_{towidth}$. Higher local position feedback degrades performance in free motion or soft contact operations.

If the transparency-optimized control law (26) is employed to select the feedforward control parameters C_1 and C_2, η_{pf} in (55) is further simplified to

$$\eta_{pf}(\omega) = \cos(\angle e^{-j2\omega T_d}) + 2\frac{1+C_6}{1+C_5}\Re\{\frac{1}{Z_{cm}}\}\Re\{Z_{cs}\}. \tag{57}$$

As a result, the system parameter changes such that in addition to the master local force feedback and slave damping, the slave local force feedback and the master local position feedback are now pivotal factors in stability robustness of the system as well. To guarantee absolute stability, $\frac{1+C_6}{1+C_5}\Re\{Z_{cs}\}\Re\{\frac{1}{Z_{cm}}\} \geq 1$ must hold, which is achievable only at midrange frequencies as $\Re\{\frac{1}{Z_{cm}}\} \rightarrow 0$ at low and high frequencies. If time delay is insignificant, then the system is always absolutely stable as $\eta_{pf} \geq 1, \forall\omega \geq 0$, and neither $Z_{tomin} \rightarrow 0$ nor $Z_{towidth} \rightarrow \infty$. This suggests that the transparency-optimized control law sacrifices stability more in the P-P and F-F architectures than in the P-F architecture.

References

Adams, R. J., and Hannaford, B. 1999. Stable haptic interaction with virtual environments. *IEEE Transactions on Robotic and Automation* 15:465–474.

Anderson, R. J., and Spong, M. W. 1989. Bilateral control of teleoperators with time delay. *IEEE Transactions of Automation and Control* 34:494–501.

Brooks, T. J. 1990. Telerobotics response requirements. *Proceedings of the IEEE International Conference on Systems, Man and Cybernetics*, pp. 113–120.

Clover, C. L., Luecke, G. R., Troy, J. J., and McNeely, W. A. 1997. Dynamic simulations of virtual mechanisms with haptic feedback using industrial robotics equipment. *Proceedings of the IEEE International Conference on Robotics and Automation*, Albuquerque, NM, pp. 724–730.

Colgate, J. E. 1993. Robust impedance shaping telemanipulation. *IEEE Transactions on Robotics and Automation* 9:374–384.

Colgate, J. E., and Brown, J. M. 1994. Factors affecting the Z-width of a haptic display. *Proceedings of the IEEE International Conference on Robotics and Automation*, San Diego, CA, pp. 3205–3210.

Colgate, J. E., and Hogan, N. 1988. Robust stability of dynamically interacting systems. *International Journal of Control* 48(1):65–88.

Daniel, R. W., and McAree, P. R. 1998. Fundamental limits of performance for force reflecting teleoperation. *International Journal of Robotics Research* 17:811–830.

Eusebi, A., and Melchiorri, C. 1998. Force reflecting telemanipulators with time-delay: Stability analysis and control design. *IEEE Transactions on Automation and Control* 14:635–640.

Handlykken, M., and Turner, T. 1980. Control system analysis and synthesis for a 6-degree-of-freedom universal force-reflecting hand controller. *Proceedings of the IEEE International Conference on Decision and Control*, Albuquerque, NM, pp. 1197–1205.

Hannaford, B. 1989a. A design framework for teleoperators with kinesthetic feedback. *IEEE Transactions on Robotics and Automation* 5:426–434.

Hannaford, B. 1989b. Stability and performance tradeoffs in bilateral telemanipulation. *IEEE Conference on Robotics and Automation*, Scottsdale, AZ, pp. 1764–1767.

Hannaford, B., and Anderson, R. J. 1988. Experimental and simulations of hard contact in force reflecting teleoperation. *Proceedings of the IEEE International Conference on Robotics and Automation*, Philadelphia, PA, pp. 584–589.

Hashtrudi-Zaad, K., and Salcudean, S. E. 1999. On the use of local force feedback for transparent teleoperation. *Proceedings of the IEEE International Conference on Robotics and Automation*, Detroit, MI, pp. 1863–1869.

Haykin, S. S. 1970. *Active Network Theory.* Reading, MA: Addison-Wesley.

Hogan, N. 1989. Controlling impedance at the man/machine interface. *Proceedings of the IEEE International Conference on Robotics and Automation*, Scottsdale, AZ, pp. 1626–1631.

Hollis, R. L., Salcudean, S. E., and Allan, A. P. 1991. A six-degree-of-freedom magnetically levitated variable impedance fine-motion wrist: Design, modelling, and control. *IEEE Transactions on Robotics and Automation* 7:320–332.

Kazerooni, H., Tsay, T.-I., and Hollerbach, K. 1993. A controller design framework for telerobotic systems. *IEEE Transactions on Control Systems Technology* 1(1):50–62.

Lawrence, D. A. 1993. Stability and transparency in bilateral teleoperation. *IEEE Transactions on Robotics and Automation* 9:624–637.

Leung, G.M.H., Francis, B. A., and Apkarian, J. 1995. Bilateral controller for teleoperators with time delay via μ-synthesis. *IEEE Transactions on Robotics and Automation* 11:105–116.

Massie, T. H., and Salisbury, J. K. 1994. The Phantom haptic interface: A device for probing virtual objects. *Proceedings of the ASME International Mechanical Engineering Congress and Exposition*, Chicago, IL, pp. 295–302.

Melchiorri, C., and Eusebi, A. 1996. Telemanipulation: System aspects and control issues. In *Proceedings of the International Summer School in Modelling and Control of Mechanisms and Robots*, ed. C. Melchiorri and A. Tornambe, 149–183. Bertinoro, Italy: World Scientific.

Niemeyer, G., and Slotine, J.-J.E. 1991. Stable adaptive teleoperation. *IEEE Journal of Oceanic Engineering* 16:152–162.

Raju, G. J., Verghese, G. C., and Sheridan, T. B. 1989. Design issues in 2-port network models of bilateral remote

manipulation. *Proceedings of the IEEE International Conference on Robotics and Automation*, Scottsdale, AZ, pp. 1316–1321.

Salcudean, S. E. 1998. Control for teleoperation and haptic interfaces. In *Control Problems in Robotics and Automation*, LNCIS-230, ed. B. Siciliano and K. P. Valavanis, 51–66. New York: Springer-Verlag.

Salcudean, S. E., Hashtrudi-Zaad, K., Tafazoli, S., DiMaio, S. P., and Reboulet, C. 1999. Bilateral matched-impedance teleoperation with application to excavator control. *Control Systems Magazine* 19(6):29–37.

Salcudean, S. E., Tafazoli, S., Hashtrudi-Zaad, K., Reboulet, C., and Lawrence, P. D. 1998. Evaluation of impedance and teleoperation control of a hydraulic mini-excavator. In *5th International Symposium on Experimental Robotics (ISER'97), Barcelona, Spain*, LNCIS-232, ed. A. Casals and A. T. de Almeida, 229–240. New York: Springer-Verlag.

Salcudean, S. E., Wong, N. M., and Hollis, R. L. 1995. Design and control of a force-reflecting teleoperation system with magnetically levitated master and wrist. *IEEE Transactions on Robotics and Automation* 11:844–858.

Salcudean, S. E., Yan, J., Hu, J., and Loewen, P. D. 1995. Performance trade-offs in optimization-based teleoperation controller design with applications to microsurgery experiments. *Proceedings of the International Mechanical Engineering Congress and Exposition*, pp. 631–640.

Yokokohji, Y., and Yoshikawa, T. 1994. Bilateral control of master-slave manipulators for ideal kinematic coupling—Formulation and experiment. *IEEE Transactions on Robotics and Automation* 10:605–620.

Yoshikawa, T., and Ueda, J. 1996. Analysis and control of master-slave systems with time delay. *Proceedings of the IEEE/RSJ International Conference on Intelligent Robots and Systems*, Osaka, Japan, pp. 1366–1373.